Pro-tumourigenic effects of DCAF13 on the progression of colorectal cancer

WENQI ZHANG[1,2*], RONGRONG ZHANG[1*], MENGXUAN JIA[1*], SHUTING LAN[1], FANGYUAN LIU[1], QIN JIN[3], LIYA SU[1] and GANG LIU[1]

[1]Central Laboratory, Clinical Medicine Research Centre, Affiliated Hospital of Inner Mongolia Medical University, Hohhot, Inner Mongolia Autonomous Region 010050, P.R. China; [2]Department of Clinical Laboratory, People's Hospital of Tianchang, Tianchang, Anhui 239300, P.R. China; [3]Department of Pathology, Affiliated Hospital of Nantong University, Nantong, Jiangsu 226001, P.R. China

Received April 17, 2025; Accepted October 2, 2025

DOI: 10.3892/ol.2026.15498

Abstract. Colorectal cancer (CRC) remains one of the most common and lethal malignancies worldwide, with limited effective biomarkers for predicting prognosis and guiding immunotherapy response. The present study aimed to investigate the potential of DDB1- and CUL4-associated factor 13 (DCAF13) as a biomarker for CRC. Bioinformatics analyses were performed using public datasets from The Cancer Genome Atlas and Gene Expression Omnibus; ESTIMATE, CIBERSORT, immune checkpoint, TIDE score and Kaplan-Meier survival analyses were performed to assess the prognostic value and implications of DCAF13 expression in CRC. *In silico* findings were validated through immunohistochemistry (IHC), *in vitro* cell-based assays and transcriptomic analysis. Increased DCAF13 expression levels were associated with reduced overall survival in patients with CRC based on the bioinformatics analysis, and this was validated using samples from patients using IHC. Immune profiling demonstrated an increased infiltration of M0 and M1 macrophages, activation of mast cells, neutrophils and $CD4^+$ memory T cells in the DCAF13-high expression group compared with the DCAF13-low expression group. DCAF13 expression was correlated with immune modulators and checkpoint genes. High DCAF13 expression was associated with lower TIDE scores. *In vitro* assays and transcriptomic analyses confirmed the pro-tumourigenic effects of DCAF13, which demonstrated roles in regulating cell proliferation, migration, clonogenicity, adhesion, metastasis, epithelial-to-mesenchymal transition and homologous recombination in CRC cells. The present study demonstrated that DCAF13 was upregulated in CRC and served a role in tumour progression, thus providing novel insights into the pro-tumourigenic functions of DCAF13 and its potential as a critical regulator in CRC.

Correspondence to: Dr Liya Su or Dr Gang Liu, Central Laboratory, Clinical Medicine Research Centre, Affiliated Hospital of Inner Mongolia Medical University, 1 Tongdao North Street, Hohhot, Inner Mongolia Autonomous Region 010050, P.R. China
E-mail: suliya2307@hotmail.com
E-mail: 20190043@immu.edu.cn

*Contributed equally

Key words: colorectal cancer, DDB1- and CUL4-associated factor 13, tumour microenvironment, immune infiltration, homologous recombination

Introduction

Colorectal cancer (CRC), a malignant neoplasm originating from the mucosal lining of the colon or rectum, remains a significant global health burden. It is often diagnosed in the first instance at an advanced stage, which complicates both treatment and prognosis (1,2). Patients typically present with systemic symptoms such as fatigue, unintended weight loss, anaemia, abdominal pain and in certain cases, fever, often indicative of metastatic spread. As a highly heterogeneous disease, CRC encompasses several subtypes, including mucinous, non-mucinous, neuroendocrine and undifferentiated forms, each characterised by distinct molecular and histological features (3). This heterogeneity poses substantial challenges for clinical management, especially in advanced disease, where resistance to conventional therapies is common and long-term survival rates remain low (4). While early detection through screening and adenoma resection has contributed to a decline in mortality, CRC incidence and metastatic potential continue to rise. Globally, >1.85 million new cases and 850,000 CRC-related mortalities are reported annually (2). Notably, China recorded ~600,000 new CRC cases and 261,777 CRC-related mortalities in 2019, the highest national mortality worldwide (5). The 5-year survival rate for metastatic CRC remains <15%, despite aggressive treatment (6). These trends are suggested to be driven by an ageing population, the widespread adoption of Western dietary habits and rising obesity, which are well-established risk factors for CRC (7-9). Collectively, these factors underscore the need for innovative approaches to CRC prevention, early diagnosis and treatment.

Current treatment strategies for CRC typically involve a combination of surgery, chemotherapy and radiation

therapy (9). Surgery remains the primary curative approach for localised CRC, while chemotherapy and radiotherapy are critical for advanced or metastatic disease. Targeted therapies, such as monoclonal antibodies against epidermal growth factor receptor (EGFR) and vascular endothelial growth factor (VEGF), have improved outcomes in specific patient subgroups, most notably patients with RAS wild-type tumours for EGFR-targeted therapy and those receiving combination chemotherapy for VEGF inhibition. EGFR inhibitors, including cetuximab and panitumumab, are effective in patients harbouring wild-type RAS genes by blocking ligand binding and downstream signalling pathways involved in tumour progression. Similarly, VEGF inhibitors such as bevacizumab suppress tumour angiogenesis, enhancing the efficacy of chemotherapy (10). However, the clinical success of these therapies is often limited by acquired resistance and immune-related complications (11).

In this context, cancer immunotherapy has emerged as a transformative modality, offering durable responses in various malignancies, including CRC (12). Immunotherapeutic strategies, such as immune checkpoint inhibitors (ICIs), adoptive cell transfer, cancer vaccines and oncolytic virus therapy, aim to reactivate antitumour immunity by targeting immune evasion mechanisms (12). Among them, ICIs have shown therapeutic potential, especially in tumours with high microsatellite instability (MSI-H) or mismatch repair deficiency (dMMR), where they can elicit sustained clinical responses (13). Nevertheless, the efficacy of ICIs in the broader CRC population remains limited. A notable proportion of patients exhibit primary or acquired resistance to ICIs, and immune-related adverse events, including dermatological, gastrointestinal, pulmonary and endocrine toxicities, are frequently observed (12,14). These challenges highlight the need for reliable immune-related biomarkers that can guide treatment selection, predict response and minimise toxicity (12).

Recent studies have implicated dysregulation of the tumour immune microenvironment as a key mechanism underlying resistance to immunotherapy (15,16). Among the emerging regulatory proteins, DDB1- and CUL4-associated factor 13 (DCAF13) has gained attention due to its multifaceted roles in oncogenesis and immune modulation. DCAF13 is a conserved substrate receptor in the CUL4-DDB1 E3 ubiquitin ligase complex, involved in post-translational modification, RNA metabolism, protein degradation and cell cycle regulation (17-19). Functionally, DCAF13 acts as a novel RNA-binding protein, with pivotal roles in zygotic genome activation and immune homeostasis (20). DCAF13 deficiency leads to impaired proliferation in HeLa cells and preimplantation lethality in murine embryos (20), while DCAF13 upregulation is associated with a poor prognosis in patients with breast cancer, where it promotes tumour progression via the NOTCH4 signalling pathway (21,22). In addition to breast cancer, DCAF13 has been associated with tumorigenesis in lung, liver, ovarian and haematological malignancies (23-26). DCAF13 also modulates immune responses within the tumour microenvironment (TME); in the TME, DCAF13 contributes to immune escape and resistance to ICIs, as demonstrated in lung adenocarcinoma and hepatocellular carcinoma (26,27). Furthermore, DCAF13 is essential for T-cell function, and it has been shown that DCAF13 depletion disrupts T-cell proliferation and homeostasis (28). These findings suggest a dual role for DCAF13 in promoting tumour progression and mediating immune evasion, making it a compelling candidate for further exploration in cancer immunotherapy.

While the oncogenic role of DCAF13 has been increasingly recognised, its specific function in CRC and association with immune infiltration remain poorly understood. Sun *et al* (29) recently demonstrated that CRISPR-mediated knockout of *DCAF13* significantly impaired CRC cell proliferation. The present study investigated the biological function of DCAF13 in CRC progression and immune modulation. Bioinformatics analyses, including ESTIMATE, CIBERSORT, immune checkpoint profiling, TIDE scoring and GEPIA, were used to explore the relationship between DCAF13 and the tumour immune microenvironment. Findings were validated using transcriptomic data from the GSE40967 dataset and immunohistochemical (IHC) staining of clinical CRC samples. *In vitro* functional assays further confirmed the oncogenic role of DCAF13. These results highlight DCAF13 as a novel immune-related biomarker and a promising therapeutic target for improving immunotherapy efficacy in CRC.

Materials and methods

Data collection and preprocessing. Gene expression profiles and associated clinical information for patients with CRC in The Cancer Genome Atlas (TCGA) cohort were obtained from the UCSC Xena database (https://xena.ucsc.edu/, accessed in March 2024). The data, with 332 primary CRC cases, were screened and samples without follow-up information, with 0-day survival or representing duplicate sequencing from the same patient were removed, which resulted in a final cohort of 282 primary CRC cases for the training dataset. The gene expression dataset GSE40967 (575 CRC samples and 10 normal tissue samples) was downloaded from the Gene Expression Omnibus (GEO) repository (https://ncbi.nlm.nih.gov/geo/) (30); this dataset served as the external validation set. Samples lacking survival data in the GSE40967 dataset were excluded from further analysis. To minimise technical variability between datasets, batch effects were corrected using the R 'limma' package (version 3.50.3) (31). Specifically, the 'removeBatchEffect' function was applied after merging tumour samples from the validation cohort in the UCSC Xena data with GSE40967, which were generated using the same microarray platform [GPL570 (HG-U133_Plus_2); Human Genome U133 Plus 2.0 Array; Affymetrix; Thermo Fisher Scientific, Inc.]. Subsequently, mRNA expression data from both datasets were normalised to ensure consistency for downstream analysis. The demographics and clinicopathological characteristics of these patients are displayed in Table I.

Pan-cancer function and expression analyses of DCAF13. Pan-cancer functional analyses of DCAF13 were performed using the Cancer Single-Cell State TCGA (CancerSEA; https://biocc.hrbmu.edu.cn/CancerSEA/) database (32). Expression levels of DCAF13 across different types of cancer were explored using the Tumor Immune Estimation Resource (TIMER; cistrome.shinyapps.io/timer/) (33), which was used to compare DCAF13 expression levels between cancer tissues and matched normal samples.

Table I. Clinical features of patients with CRC in the TCGA (n=332) and GEO (n=585) datasets.

Clinical feature	TCGA, n (%)	GSE40967, n (%)
Overall survival		
Alive	276 (83.13)	385 (65.81)
Dead	56 (16.87)	195 (33.33)
Age, years		
>58	238 (71.69)	441 (75.38)
≤58	94 (28.31)	141 (24.10)
Sex		
Male	180 (54.22)	322 (55.04)
Female	152 (45.78)	263 (44.96)
PR status		
Positive	-	395 (67.52)
Negative	-	180 (30.77)
Indeterminate	-	11 (1.89)
Stage		
I	106 (31.93)	38 (6.50)
II	84 (25.30)	271 (46.32)
III	92 (27.71)	210 (35.90)
IV	50 (15.06)	60 (10.26)
T stage		
T1	18 (5.42)	12 (2.05)
T2	56 (16.87)	49 (8.38)
T3	228 (68.67)	379 (64.79)
T4	28 (8.43)	119 (20.34)
N stage		
N0	168 (50.60)	314 (53.68)
N1	90 (27.11)	137 (23.42)
N2	68 (20.48)	100 (17.09)
M stage		
M0	252 (75.90)	499 (85.30)
M1	48 (14.49)	61 (10.43)

CRC, colorectal cancer; DACF13, DDB1- and CUL4-associated factor 13; TCGA, The Cancer Genome Atlas.

For prognostic analysis, patients in the data from TCGA (https://www.cancer.gov/ccg/research/genome-sequencing/tcga) were stratified into high- and low-expression groups based on the median expression levels of DCAF13, which served as the optimal cut-off value. The median DCAF13 expression was 11.98325, with patients exhibiting expression levels ≥11.98325 classified into the high-expression group, and those <11.98325 into the low-expression group. The association between DCAF13 expression and overall survival (OS) was evaluated using Kaplan-Meier (KM) survival analysis via the Kaplan-Meier Plotter online tool (http://gepia.cancer-pku.cn/), using the CRC mRNA dataset. Patients were stratified into high- and low-expression groups based on the median expression of DCAF13, and OS was analysed using the log-rank test. The findings were validated using the GSE40967 dataset by performing the same survival analysis on this external cohort, with patients stratified into high- and low-expression groups based on the median DCAF13 expression level within the GSE40967 cohort.

Assessment of immune cell infiltration, immune checkpoints and response to immunotherapy. To assess immune cell infiltration and immune checkpoint activity, several computational tools and bioinformatics algorithms were used. The ESTIMATE algorithm (https://bioinformatics.mdanderson.org/estimate/) was used to evaluate the stromal (StromalScore, SS), immune (ImmuneScore, IS), and overall ESTIMATE scores for each tumour sample in the data from TCGA (34). These scores were derived from gene expression data using the ESTIMATE R package (version 1.0.13). The relationships between DCAF13 expression and the SS, IS, and ESTIMATE scores were further analysed to gain insights into its role in immune regulation within the TME.

For further assessment of immune infiltration, the CIBERSORT software (https://sangerbox.com; accessed in March 2024) was used to estimate the relative proportions of 22 immune cell types in each tumour sample. This was achieved through the analysis of a normalised gene expression matrix (35). Differences in immune infiltration between the high- and low-DCAF13 expression groups were compared using the Wilcoxon rank-sum test (two-sided).

To explore the role of DCAF13 in regulating cancer immunity, its correlation with various immune checkpoints, including B and T lymphocyte attenuator (BTLA), lymphocyte-activating 3 (LAG-3), signal regulatory protein α (SIRPα) and V-domain Ig suppressor of T-cell activation (VISTA) was visualised using Gene Expression Profiling Interactive Analysis (GEPIA; https://gepia.cancer-pku.cn/) (36). Additionally, the correlation between DCAF13 expression and 122 immune checkpoint-related genes (ICPs) was analysed using Pearson's correlation analysis (37).

To predict the response to immunotherapy, Tumor Immune Dysfunction and Exclusion (TIDE; https://tide.dfci.harvard.edu/; accessed in March 2024) analysis was applied to the high- and low-DCAF13 expression groups (38). In the present study, the TIDE score, dysfunction score, exclusion score and MSI score between the high- and low-DCAF13 expression groups were calculated to evaluate their potential responsiveness to immunotherapy.

Patient specimens and ethics statement. In the present study, a total of 234 paraffin-embedded CRC tissue samples and their matched adjacent non-tumorous tissues, collected ≥5 cm away from the tumour margin, were obtained from patients who underwent surgical resection at the Department of Pathology, Affiliated Hospital of Inner Mongolia University (Hohhot, China) between January 2013 and June 2015. All samples were histologically confirmed as CRC and were obtained prior to any neoadjuvant therapy. Among the 234 patients, 146 were male and 88 were female. The age distribution showed 83 patients were aged ≤60 years and 151 patients were aged >60 years. The cohort included tumours originating from both the colon and rectum, including the ascending (n=76), transverse (n=31), descending/sigmoid (n=68) colon and rectum (n=59). Tumour histology was classified according to WHO

Table II. Association of DCAF13 expression with clinical characteristics and biological markers of patients with CRC.

Characteristic	Patients, n	High-DCAF13 expression (n=137), n (%)	Low- or no-DCAF13 expression (n=97), n (%)	χ^2	P-value
Age, years				0.994	0.319
≤60	83	45 (54.2)	38 (45.8)		
>60	151	92 (60.9)	59 (39.1)		
Sex				0.164	0.685
Male	146	84 (57.5)	62 (42.5)		
Female	88	53 (60.2)	35 (39.8)		
Tumour size, cm				2.012	0.156
≤5	182	111 (61.0)	71 (39.0)		
>5	52	26 (50.0)	26 (50.0)		
Histological classification				0.563	0.453
Tubular + papillary	208	120 (57.7)	88 (42.3)		
Other	26	17 (65.4)	9 (34.6)		
Location				6.712	0.082
Ascending colon	76	44 (57.9)	32 (42.1)		
Transverse colon	31	18 (58.1)	13 (41.9)		
Descending + sigmoid colon	68	33 (48.5)	35 (51.5)		
Rectum	59	42 (71.2)	17 (28.8)		
Differentiation				4.080	0.043
Well + moderate	141	90 (63.8)	51 (36.2)		
Poor	93	47 (50.5)	46 (49.5)		
T stage				4.158	0.125
T1	54	28 (51.9)	26 (48.1)		
T2	100	55 (55.0)	45 (45.0)		
T3 + T4	80	54 (67.5)	26 (32.5)		
N stage				2.099	0.350
N0	141	84 (59.6)	57 (40.4)		
N1	63	39 (61.9)	24 (38.1)		
N2	30	14 (46.7)	16 (53.3)		
TNM stage				8.310	0.016
I	26	12 (46.2)	14 (53.8)		
II	62	29 (46.8)	33 (53.2)		
III + IV	146	96 (65.8)	50 (34.2)		

CRC, colorectal cancer; DACF13, DDB1- and CUL4-associated Factor 13.

criteria, with the majority being tubular or papillary adenocarcinomas (n=208), and the rest categorised as other types (n=26) (39). Tumour differentiation included well/moderately differentiated (n=141) and poorly differentiated (n=93) tumours. Staging was based on the AJCC 8th edition TNM classification, comprising stage I (n=26), stage II (n=62) and stage III/IV (n=146) cases (40). Additional T and N staging details were also recorded. The present study was approved by the Ethical Review Committee of Inner Mongolia Medical University (approval no. 2022513411; Hohhot, China) and was performed in accordance with the Declaration of Helsinki. Informed consent was written from all patients prior to inclusion in the study. Detailed clinicopathological characteristics are summarised in Table II.

Immunohistochemical (IHC) staining. All tissue samples were fixed in 10% neutral-buffered formalin (no. G2161; Beijing Solarbio Science & Technology Co., Ltd.) at room temperature for 24 h, routinely dehydrated, embedded in paraffin and stored under standard conditions. No tissues were frozen after paraffin embedding. Prior to use, the paraffin sections of the 234 CRC samples and their adjacent tissues were prepared at a thickness of 4 μm, deparaffinised in xylene, rehydrated through a graded ethanol series and washed with PBS (0.01 M, pH 7.0) (41). Endogenous peroxidase activity was quenched by incubation with 3% hydrogen peroxide (cat. no. H792073; Shanghai Macklin Biochemical Co., Ltd.) at room temperature for 10 min. Antigen retrieval was performed by boiling the slides in citrate buffer (0.01 M, pH 6.0) at 95-100˚C for

15 min, followed by natural cooling to room temperature. For blocking of non-specific binding, the sections were incubated with 5% goat serum (cat. no. SL039; Beijing Solarbio Science & Technology Co., Ltd.) at 37˚C for 30 min. The sections were then incubated at 4˚C overnight with a rabbit anti-DCAF13 antibody (1:500; cat. no. bs-62879R; BIOSS). After washing with PBS, the sections were incubated with a goat anti-rabbit HRP secondary antibody (1:2,000; cat. no. ZDR-5306; Beijing Zhongshan Jinqiao Biotechnology Co., Ltd.) at 37˚C for 1 h. For visualisation, the sections were incubated with DAB chromogen (cat. no. DA1010, Beijing Solarbio Science & Technology Co., Ltd.) at room temperature for 5 min, followed by counterstaining with haematoxylin solution at room temperature for 10 sec. Immunostained sections were independently evaluated by two experienced pathologists under blinded conditions using a light microscope (Olympus BX53; Olympus Corporation).The staining intensity and percentage of DCAF13-positive cells were quantitatively analysed using ImageJ software (version 1.53t; National Institutes of Health).

Cell culture. FHC, Caco2, SW480, HCT116, Lovo and RKO cells were used in the present study and cultured in a humidified atmosphere at 37˚C and 5% CO_2. FHC cells, a normal intestinal cell line, were purchased from Zhejiang Meisen Cell Technology Co., Ltd. (cat. no. CTCC-001-0208) and cultured in their respective commercial medium (cat. no. CTCC-002-047; Zhejiang Meisen Cell Technology Co., Ltd). Caco2 cells were cultured in MEM medium (cat. no. PM150410; Procell Life Science & Technology Co., Ltd.) supplemented with 20% foetal bovine serum (FBS; cat. no. C04001; Shanghai VivaCell Biosciences, Ltd.) and 100 IU/ml penicillin/streptomycin (P/S; cat. no. 15070063; Thermo Fisher Scientific, Inc.). SW480, Lovo and RKO cells were cultured in DMEM medium (cat. no. PM150210; Procell Life Science & Technology Co., Ltd.) with 10% FBS and 100 IU/ml P/S. HCT116 cells were maintained in IMEM medium (cat. no. C12440500BT; Gibco; Thermo Fisher Scientific, Inc.) supplemented with 10% FBS and 100 IU/ml P/S.

Western blotting. To identify the CRC cells with the highest expression levels of DCFA13, protein lysates from CRC cells were extracted using RIPA lysis buffer (cat. no. DE101; TransGen Biotech Co., Ltd.) and quantified using a bicinchoninic acid assay kit (cat. no. PC0020; Beijing Solarbio Science & Technology Co., Ltd.) (42,43). Proteins (30 μg per lane) were resolved by 10% SDS-PAGE (cat. no. P1200; Beijing Solarbio Science & Technology Co., Ltd.) and transferred to PVDF membranes (cat. no. PVH00010; Merck KGaA) using 1x Tris-glycine buffer (cat. no. G2145; Wuhan Servicebio Technology Co., Ltd.). After blocking with 10% non-fat milk at room temperature for 1 h, the membranes were incubated at 4˚C overnight with a rabbit anti-DCAF13 antibody (1:2,000; cat. no. bs-62879R; BIOSS), a rabbit anti-γ-H2AX antibody (1:2,000; cat. no. ab81299; Abcam), a rabbit anti-ATM antibody (1:2,000; cat. no. bsm-52360R; BIOSS), a rabbit anti-E-cadherin antibody (1:2,000; cat. no. AF0131; Affinity Biosciences), a rabbit anti-N-cadherin antibody (1:2,000; cat. no. AF6710; Affinity Biosciences), a rabbit anti-Vimentin antibody (1:2,000; cat. no. 60330-1-Ig; Proteintech Group, Inc.), a rabbit anti-PCNA antibody (1:2,000; cat. no. 10205-2-AP; Proteintech Group, Inc.) or a mouse anti-actin antibody (1:2,000; cat. no. CW0096M; Jiangsu CoWin Biotech Co., Ltd.). After three washes with Tris-HCl with 0.1% Tween-20, the membranes were incubated with goat anti-rabbit IgG H&L HPR antibodies (1:2,000; cat. no. S0001; Affinity Biosciences) or HRP-conjugated Affinipure goat anti-mouse IgG (1:2,000; cat. no. SA00001-1; Proteintech Group, Inc.) at room temperature for 1 h. Immunoblots were visualised using enhanced chemiluminescence (cat. no. W1001; Promega Corporation) using a ChampChemi system (Shanghai Champ Biomedical Technology Co., Ltd.). The densitometry analysis of the protein bands was performed using ImageJ software (version 1.53t; National Institutes of Health).

Lentivirus packaging and infection. Lentiviral vectors expressing either a short hairpin RNA (shRNA) targeting the DCAF13 coding region (5'-CGAATCTTTCCTGTAGAC AAA-3') or a non-targeting control shRNA sequence (5'-TTC TCCGAACGTGTCACGT-3'), which does not match any known human gene, were supplied by Shanghai GeneChem Co., Ltd. The lentiviral plasmid containing the shRNA was packaged using a second-generation system, with 293T cells (American Type Culture Collection) used as the interim cell line. For transfection, 10 μg lentiviral plasmid was mixed with 10 μg lentivirus packaging plasmid (pMD2.G) and 10 μg packaging plasmid (psPAX2) in a 1:1:1 ratio. The mixture was transfected into 293T cells using Lipofectamine 3000 (cat. no. L3000008; Thermo Fisher Scientific, Inc.) according to the manufacturer's protocol. Transfection was carried out at 37˚C for 6 h, and the medium was replaced with fresh growth medium after 6 h. Lentiviral particles were collected 48 h post-transfection, and the multiplicity of infection was adjusted to 5 for infection of RKO cells with high baseline expression of DCAF13. The cells were transduced in the presence of polybrene (8 μg/ml; cat. no. H9268; Sigma-Aldrich; Merck KGaA) for 12 h. Following transduction, cells were selected with puromycin (1 μg/ml; cat. no. 314Y0415; Beijing Solarbio Science & Technology Co., Ltd.) for 14 days to establish stable cell lines. Stable DCAF13 knockdown (shDCAF13) and the non-targeting control (shNC) cell lines were validated using RT-qPCR and western blotting.

RNA extraction and reverse transcription-quantitative PCR (RT-qPCR). RNA extraction and qPCR were performed to assess the efficiency of DCAF13 knockdown. Total RNA was extracted from RKO cells in both experimental groups using TRIzol® reagent (cat. no. 79306; Thermo Fisher Scientific, Inc.) according to the manufacturer's protocol. Reverse transcription of 1 μg of RNA was performed using a PrimeScript™ RT Reagent Kit (cat. no. RR047A; Takara Biotechnology Co., Ltd.), according to the manufacturer's protocol, to synthesise cDNA. For amplification, specific forward and reverse primers for *DCAF13* were designed using PrimerBank (version 2.1; https://pga.mgh.harvard.edu/primerbank/) and synthesised by Sango Biotech Co., Ltd. qPCR was performed using the SYBR® Premix Ex Taq™ Kit (cat. no. RR820A; Takara Biotechnology Co., Ltd.) in a 20-μl reaction volume, using a Roche LightCycler 480 II System (Roche Diagnostics). The following thermocycling conditions were used for qPCR: Initial denaturation at 94˚C for 2 min; 40 cycles of denaturation

at 95˚C for 5 sec; annealing at 60˚C for 15 sec; and extension at 72˚C for 10 sec. Fluorescence signals were detected during the annealing-extension phase, and *GAPDH* was used as the internal reference for normalisation. The relative expression levels of *DCAF13* in each group were calculated using the $2^{-\Delta\Delta Cq}$ method (44). The following primer pairs were used for qPCR: *DCAF13* forward (F), 5'-ACTGCACAGCTAAAG AACCG-3' and reverse (R), 5'-TCCCAGACTACTTCCAGT CAC-3'; and *GAPDH* F, 5'-TGAACGGGAAGCTCACTG-3' and R, 5'-GCTTCACCACCTTCTTGATG-3'.

In vitro functional assays of DCAF13 in RKO cells

Proliferation assays. RKO cells ($1x10^4$ cells per well) from both groups were seeded in a 96-well plate and imaged at 8, 16 and 24 h using an IncuCyte system (Essen Bioscience) to track proliferation. The growth curves of each group were then analysed. In addition, the expression levels of PCNA in RKO cells of both groups were detected by western blotting (42,45).

Wound healing assay. shNC and shDCAF13 RKO cells ($2x10^3$ cells) were seeded into 6-well plates and cultured at 37˚C in DMEM medium supplemented with 10% FBS and 100 IU/ml P/S overnight. A wound was created by scratching the monolayer with a 200 μl pipette tip, and the cells were cultured in DMEM medium without FBS or P/S for an additional 24 h. The degree of wound closure was observed and microscopically (Eclipse Ts2 inverted phase contrast microscope; Nikon Corporation) imaged with the cell migration rate calculated using the following formula: Migration rate (%)=[(initial wound width-wound width at 24 h)/initial wound width] x 100% (42,45).

Transwell assay. shNC and shDCAF13 RKO cells ($2x10^3$ cells) were seeded into the upper chamber of a Transwell migration assay plate (cat. no. CLS3422; Corning, Inc.) without Matrigel precoating. The medium in the upper chamber was MEM medium (cat. no. PM150410; Procell system) without serum. In the lower chamber, DMEM medium (cat. no. PM150210; Procell system) was supplemented with 20% FBS to attract migrating cells. After 24 h incubation at 37˚C, non-migrating cells on the upper side of the membrane were removed with a cotton swab, and the migrating cells on the lower membrane were fixed in 4% methanol (cat. no. P1110; Beijing Solarbio Science & Technology Co., Ltd.) at room temperature for 15 min and stained with 0.1% crystal violet (cat. no. C0121; Beyotime Biotechnology) at room temperature for 15 min. Cells were examined using an inverted phase contrast microscope (Eclipse Ts2; Nikon Corporation) at 400x magnification. A total of four fields of view per chamber were randomly selected for quantification (42,45).

Clonogenicity assay. shNC and shDCAF13 RKO cells ($1x10^3$ cells) were plated into 6-well plates and cultured for 7 days at 37˚C in DMEM medium supplemented with 10% FBS and 100 IU/ml P/S. The media was changed every 2 days. After 7 days incubation, cells were fixed with 4% paraformaldehyde (cat. no. P1110; Beijing Solarbio Science & Technology Co., Ltd.) at room temperature for 15 min, colonies were stained with 0.1% crystal violet at room temperature for 15 min. Colonies, defined as clusters of >50 cells, were examined using an inverted phase contrast microscope (Eclipse Ts2; Nikon Corporation) and counted using the Image J software (version 1.53t; National Institutes of Health) (42,45).

Adhesion assay. shNC and shDCAF13 RKO cells ($5x10^3$ cells) were plated in 10 μg/ml fibronectin-coated (precoated at 37˚C for 1 h) 96-well plates. After 30 min plating at 37˚C, the wells were washed with PBS to remove non-adherent cells. Adherent cells were fixed with 100% methanol at room temperature for 15 min and stained with 0.1% crystal violet at room temperature for 15 min. Adherent cells were examined using an inverted phase contrast microscope (Eclipse Ts2; Nikon Corporation) and counted using the Image J software (version 1.53t) (42,45).

Cell cycle analysis. shNC and shDCAF13 RKO cells were fixed overnight in 70% ethanol at 20˚C. Following the manufacturer's protocol, cells were then stained with the cell cycle analysis working solution (cat. no. CA1510; Beijing Solarbio Science & Technology Co., Ltd.) at room temperature for 1 h. The staining solution contained propidium iodide (PI; cat. no. C0121; Beyotime Biotechnology) for DNA content analysis, and RNase A (cat. no. C1608; Beyotime Biotechnology) was used to degrade RNA prior to PI staining. Intracellular permeabilization was not required in this assay, as the fixation process with ethanol preserved the cell membranes. Cell cycle analysis was performed using flow cytometry with a FACScan flow cytometer (BD Biosciences) equipped with a 488 nm laser for excitation. PI fluorescence was detected at 620 nm (FL3 channel). Data were analysed using FlowJo software (version 10.8.1; BD Biosciences) (42,45).

Transcriptomic analysis and validation. For transcriptomic analysis, total RNA was extracted from RKO cells using TRIzol® reagent (cat. no. 79306; Thermo Fisher Scientific, Inc.) according to the manufacturer's instructions (46). RNA quality and integrity were assessed using an Agilent 2100 Bioanalyzer (Agilent Technologies, Inc.), and only samples with an RNA integrity number (RIN) ≥7.0 were used for subsequent library construction. mRNA was enriched using Oligo(dT) beads, fragmented into short fragments, and reverse-transcribed into cDNA using the NEBNext® Ultra™ RNA Library Prep Kit for Illumina® (cat. no. 7530; New England BioLabs, Inc.). The resulting double-stranded cDNA fragments were end-repaired and ligated to Illumina sequencing adapters, followed by purification using AMPure XP Beads (1.0x; Beckman Coulter, Inc.) and PCR amplification. The final libraries were quantified using a Qubit™ 4 Fluorometer (Thermo Fisher Scientific, Inc.), and molar concentrations were calculated. Libraries were diluted to a final loading concentration of 8 pM prior to sequencing. Sequencing was performed on an Illumina NovaSeq 6000 platform (Illumina, Inc.) using paired-end sequencing with a read length of 150 bp (PE150). Raw sequencing data were pre-processed using fastp (version 0.18.0; https://github.com/OpenGene/fastp) to remove adapter sequences and low-quality reads. Clean reads were aligned to the human reference genome (GRCh38) using HISAT2 (version 2.4; https://daehwankimlab.github.io/hisat2/). Transcript abundance was quantified using RSEM (version 1.3.3; https://deweylab.github.io/RSEM/). Differentially expressed genes (DEGs) were identified using DESeq2 (version 1.40.2; https://bioconductor.org/packages/DESeq2/), with a false discovery rate (FDR)-adjusted P value <0.05 and an absolute $\log_2$ fold change ≥1 considered statistically significant. Functional enrichment analyses were performed using DAVID Bioinformatics Resources

(version 6.8; https://david.ncifcrf.gov/). In addition, gene set enrichment analysis (GSEA) was conducted using GSEA software (version 4.3.2; Broad Institute; https://www.gsea-msigdb.org/gsea/) to identify significantly enriched biological processes and signalling pathways associated with DCAF13 regulation.

Statistical analysis. Statistical analyses were performed using SPSS (version 19.0; IBM Corp.) and R (version 4.3.1; Posit Software, PBC). Pearson's χ^2 test was used to examine the associations between categorical variables, including DCAF13 expression status (high vs. low) and clinicopathological parameters. Pearson's correlation coefficient (r) was used to assess correlations between continuous variables, including DCAF13 expression levels and immune-related gene expression or immune infiltration scores. Differences between two independent groups were analysed using the Wilcoxon rank-sum test (Mann-Whitney U test). Kaplan-Meier survival curves were generated and compared using the log-rank test. Variables with prognostic significance in univariate analysis were further analysed using multivariate Cox proportional hazards regression. A two-sided P<0.05 was considered to indicate a statistically significant difference.

Results

Pan-cancer analysis of DCAF13 expression levels and prognostic performance in CRC. DCAF13 expression was negatively correlated with angiogenesis (r=-0.29; P<0.05) and differentiation (r=-0.30; P<0.05) signatures in CRC samples (Fig. 1A). TIMER analysis indicated that DCAF13 expression levels were significantly elevated in CRC tissues compared with that of normal colorectal samples. Additionally, compared with adjacent normal tissues, DCAF13 mRNA expression levels were increased in 18 other types of cancer (Fig. 1B).

DCAF13 was found to be significantly upregulated in CRC tumour tissue compared with that in the paired adjacent normal tissue, in both the TCGA (P<0.005; Fig. 1C) and GSE40967 validation datasets (P<0.005; Fig. 1D). KM analysis of TCGA data showed that patients with CRC with high expression levels of DCAF13 had a shorter OS [hazard ratio (HR)=1.63; P<0.05; Fig. 1E] compared with that of the low expression group. Similarly, KM analysis of the GSE40967 validation dataset confirmed that patients with CRC with high expression levels of DCAF13 had a shorter OS compared with that of the low expression group (HR=1.91; P<0.005; Fig. 1F).

Immune infiltration, immune checkpoints and response to immunotherapy. DCAF13 expression exhibited a significant negative association with both SS (P<0.05; Fig. 2A) and IS (P<0.005; Fig. 2B) in TCGA-COAD cohort after excluding samples with missing transcriptomic or ESTIMATE score data. Immune infiltration analysis using the CIBERSORT algorithm demonstrated the proportions of the 22 immune cell types in the TME of CRC in TCGA cohort (Fig. 2C). Comparison of immune cell infiltration between the high- and low-DCAF13 expression groups showed that macrophages (M0 and M1), activated mast cells, neutrophils and activated $CD4^+$ T cells were significantly more prevalent in the high-DCAF13 expression group. Conversely, the infiltration levels of naive B cells, resting dendritic cells, monocytes, plasma cells, resting $CD4^+$ T cells and $CD8^+$ T cells were significantly lower in the high-DCAF13 expression group (Fig. 2D).

Correlation between DCAF13 and immune checkpoints. Using the GEPIA database, the correlation between DCAF13 and various immune checkpoints was evaluated. The results indicated a potential association between DCAF13 and immune checkpoints, including BTLA (P<0.05; Fig. 3A), LAG-3 (P<0.05; Fig. 3B), SIRPα (P<0.05; Fig. 3C) and VISTA (P<0.05; Fig. 3D). This association with immune checkpoints led to further investigation into the relationship between DCAF13 and immunomodulators. ICP analysis demonstrated that DCAF13 expression was significantly correlated with a large proportion of immunomodulators in CRC (Fig. 3E).

TIDE score and response to immunotherapy. To predict the potential response of patients with CRC to immunotherapy, the TIDE algorithm was applied to compare predicted immunotherapy responses between patients stratified into high- and low-DCAF13 expression groups. The analysis demonstrated significantly higher TIDE scores in the high-risk group, suggesting that patients with high DCAF13 expression may have a worse response to immunotherapy compared with those in the low-risk group (P<0.05; Fig. 4A). Notably, there was no significant difference in T-cell dysfunction scores between the high- and low-risk groups; however, T-cell exclusion scores were significantly increased in the high-risk group, which indicated a greater potential for immune evasion in high-risk patients (Fig. 4B and C). Additionally, the high-risk group exhibited significantly increased MSI scores, which suggested that the high-risk CRC group may have a higher prognostic potential and poor immunotherapy response (Fig. 4D).

Upregulated expression of DCAF13 is predictive of a poor prognosis in patients with CRC. DCAF13 expression was predominantly localised to the cytoplasm in CRC tissues, whereas no notably high positive staining was observed in normal colon tissue (Fig. 5A). Quantitative analysis using the χ^2 test demonstrated that high DCAF13 expression was detected in 58.55% (137/234) of CRC tissues, significantly higher compared with the 41.45% (97/234) of non-cancerous tissues (P<0.05; Table II). Further investigation into the association between DCAF13 expression and the clinicopathological features of patients with CRC is presented in Table II. Elevated DCAF13 expression was significantly associated with poorer differentiation and advanced TNM stage in patients with CRC. Specifically, patients with well or moderately differentiated tumours exhibited a higher proportion of high DCAF13 expression (63.8%) compared with those with poorly differentiated tumours (50.5%; P<0.05; Table II), indicating a negative association between DCAF13 expression and tumour differentiation. In terms of TNM stage, high DCAF13 expression was more frequent in advanced stages (65.8% in stage III + IV vs. 46.2% in stage I; P<0.05; Table II), suggesting a positive association between DCAF13 expression and disease progression. However, no significant associations were observed between DCAF13 expression and clinicopathological factors such as age, sex, tumour location or tumour size.

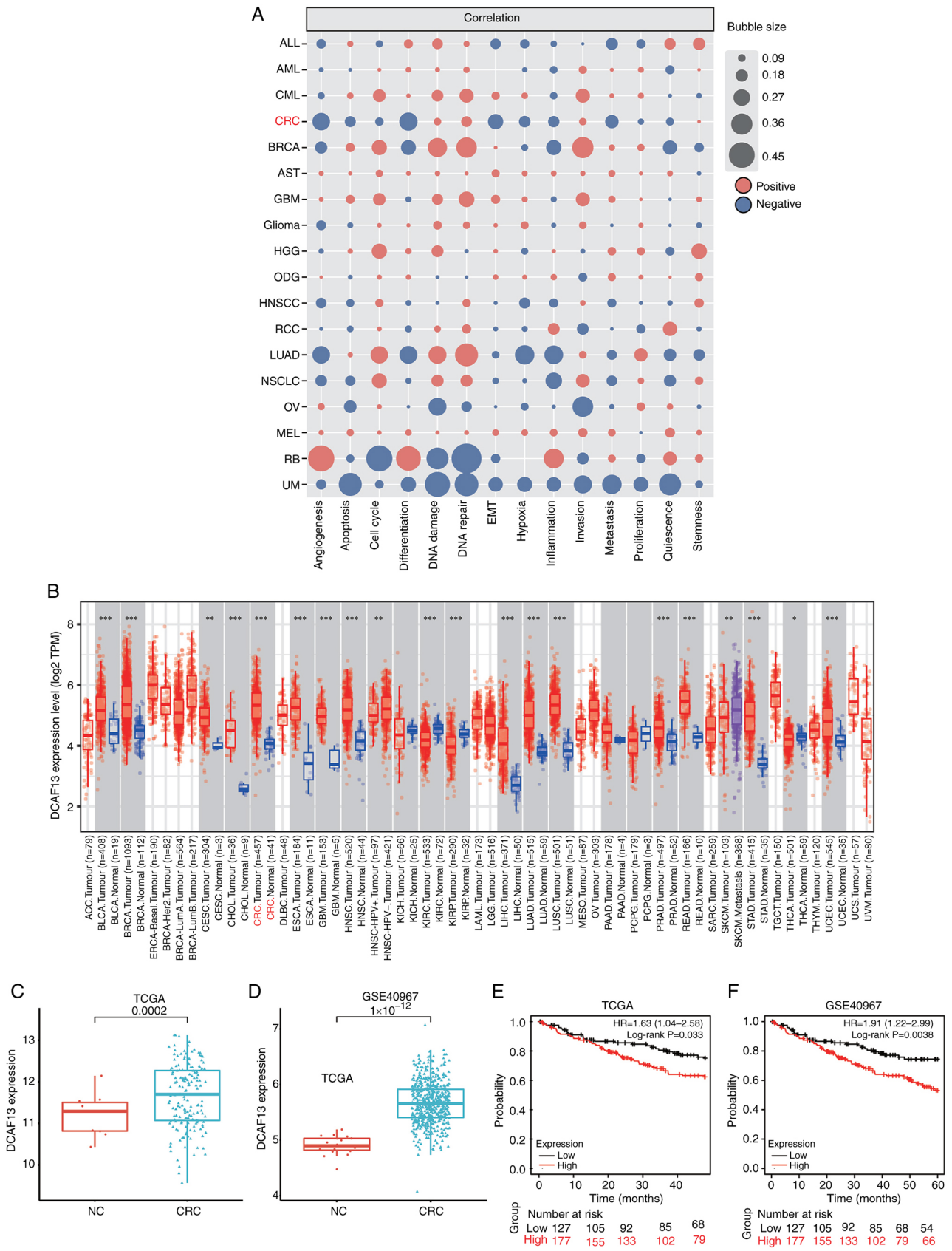

Figure 1. DCAF13 is upregulated in pan-cancer dataset and involved in multiple biological processes. (A) Functional states of DCAF13 and association with 15 different cancer types, as analysed using the CancerSEA database. (B) Expression levels of DCAF13 across various cancer types, based on data from the TCGA database and analysed using the Tumour Immune Estimation Resource tool. (C) Differential expression of DCAF13 between CRC and NC tissues in the TCGA cohort. (D) Differential expression of DCAF13 between CRC and NC tissues in the GSE40967 validation dataset. (E) KM survival analysis comparing high- and low-expression groups of DCAF13 in the TCGA cohort. (F) KM survival analysis comparing high- and low-expression groups of DCAF13 in the GSE40967 validation dataset. *P<0.05, **P<0.01 and ***P<0.001. For box plots, the centre line indicates the median, the box represents the interquartile range and the whiskers represent data dispersion. CRC, colorectal cancer; DACF13, DDB1 And CUL4 Associated Factor 13; TCGA, The Cancer Genome Atlas; KM, Kaplan-Meier; HR, hazard ratio; NC, normal control.

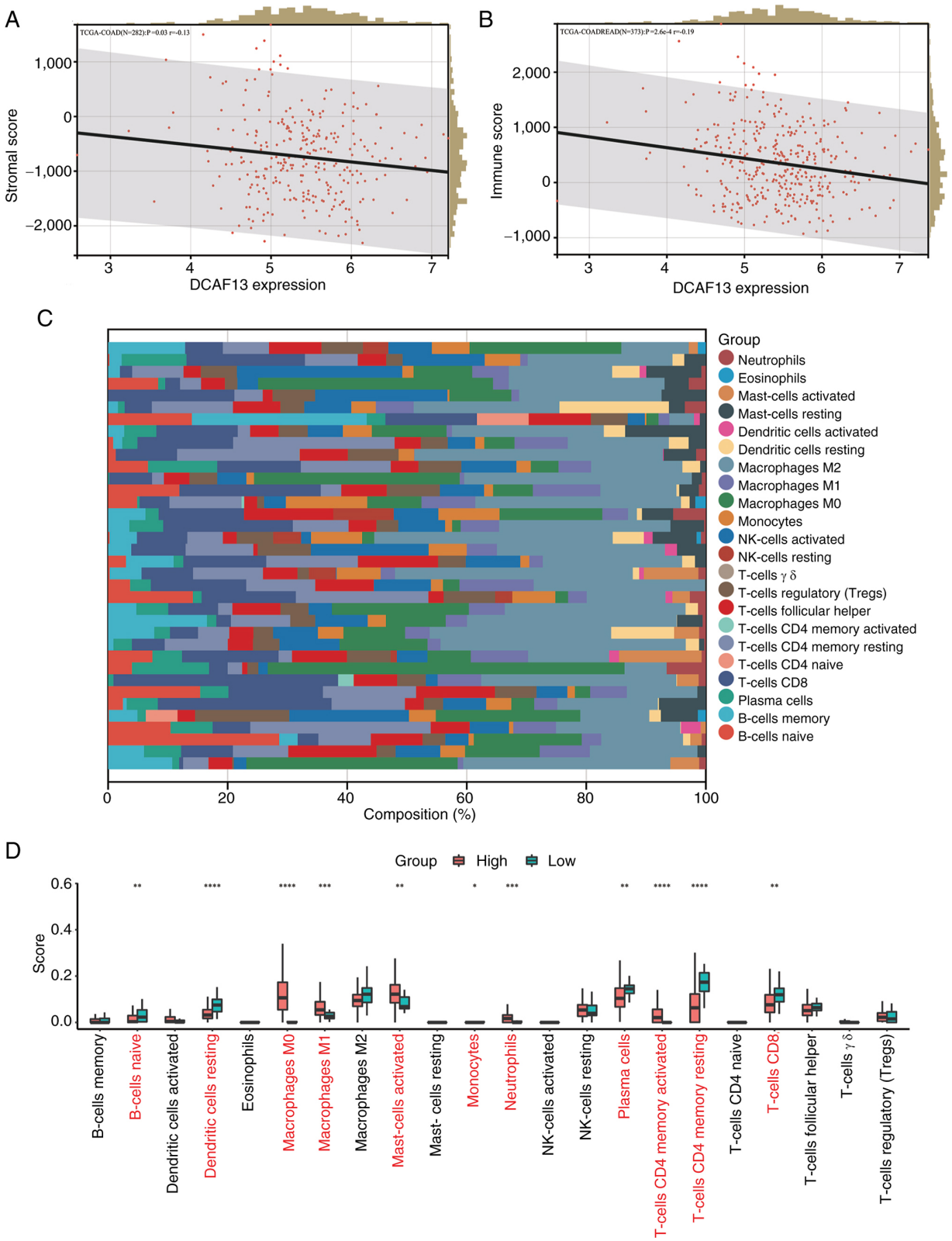

Figure 2. Distribution of ESTIMATE scores and analysis of TIICs by CIBERSORT. (A) The stromal scores of DCAF13 were calculated using the ESTIMATE method in the TCGA cohort. (B) The immune scores of DCAF13 were calculated using the ESTIMATE method in the TCGA cohort. (C) Bar chart depicting the proportion of 22 TIIC types in the TME of CRC. (D) Boxplot comparing the distribution of 22 TIICs in the TME of CRC between high- and low-DCAF13 expression groups. Red labels indicate immune cell subtypes showing statistically significant differences between the high and low DCAF13 expression groups. *P<0.05, **P<0.01, ***P<0.001 and ****P<0.0001. CRC, colorectal cancer; DACF13, DDB1- and CUL4-associated factor 13; TCGA, The Cancer Genome Atlas; TIIC, tumour-infiltrating immune cells; TME, tumour microenvironment.

To evaluate the clinical relevance of DCAF13 expression, univariable analyses were performed to assess its relationship with various clinicopathological factors (Table III). High DCAF13 expression (HR=2.230; P<0.001) and advanced

Table III. Univariate and multivariate analysis of prognostic factors in CRC for 5-year overall survival.

Parameter	Variable	Univariate analysis			Multivariate analysis		
		HR	P-value	95% CI	HR	P-value	95% CI
Expression of DCAF13	High-expression vs. low- or no-expression	2.230	<0.001[a]	1.504-3.305	2.148	<0.001	1.447-3.189
Age, years	≤60 vs. >60	0.962	0.840	0.663-1.396			
Sex	Male vs. female	0.749	0.134	0.512-1.094			
Tumour size, cm	≤5 vs. >5	0.936	0.768	0.603-1.453			
Histological classification	Tubular + papillary vs. other	1.106	0.723	0.633-1.931			
Location	Ascending colon vs. transverse colon vs. descending colon vs. sigmoid colon vs. rectum	0.913	0.240	0.785-1.062			
Differentiation	Well + moderate vs. poor	0.899	0.562	0.626-1.289			
T stage	T1 vs. T2 vs. T3 + T4	1.214	0.105	0.960-1.535			
N stage	N0 vs. N1 vs. N2	1.202	0.128	0.949-1.523			
TNM stage	I vs. II vs. III + IV	1.464	0.010[a]	1.096-1.955	1.398	0.023	1.047-1.867

[a]P<0.05 was considered to indicate a statistically significant difference. CRC, colorectal cancer; DACF13, DDB1- and CUL4-associated Factor 13; HR, hazard ratio.

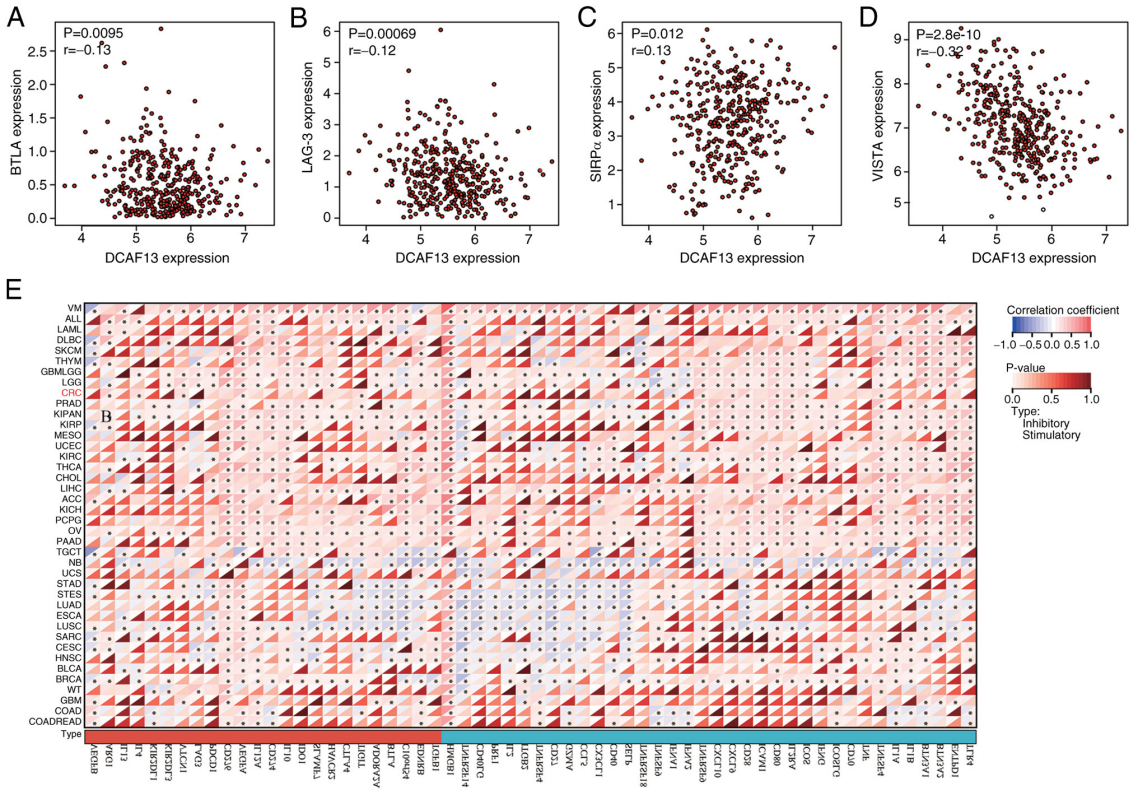

Figure 3. Correlation between DCAF13 and immune checkpoints and immune checkpoint gene analysis. (A) Correlation between DCAF13 expression and BTLA. (B) Correlation between DCAF13 expression and LAG-3. (C) Correlation between DCAF13 expression and SIRPα. (D) Correlation between DCAF13 expression and VISTA. (E) Correlation analysis between different types of cancer, including CRC, and 122 immunomodulators, including chemokines, receptors, MHC molecules and immunostimulators. *P<0.05. DACF13, DDB1- and CUL4-associated factor 13; BTLA, B and T lymphocyte attenuator; LAG-3, lymphocyte-activating 3; SIRPα, signal regulatory protein α; VISTA, V-domain Ig suppressor of T-cell activation.

TNM stage (HR=1.464; P<0.05) were significantly associated with a worse OS in patients with CRC. Multivariable Cox proportional hazards regression analysis confirmed that high DCAF13 expression (HR=2.148; P<0.001) and

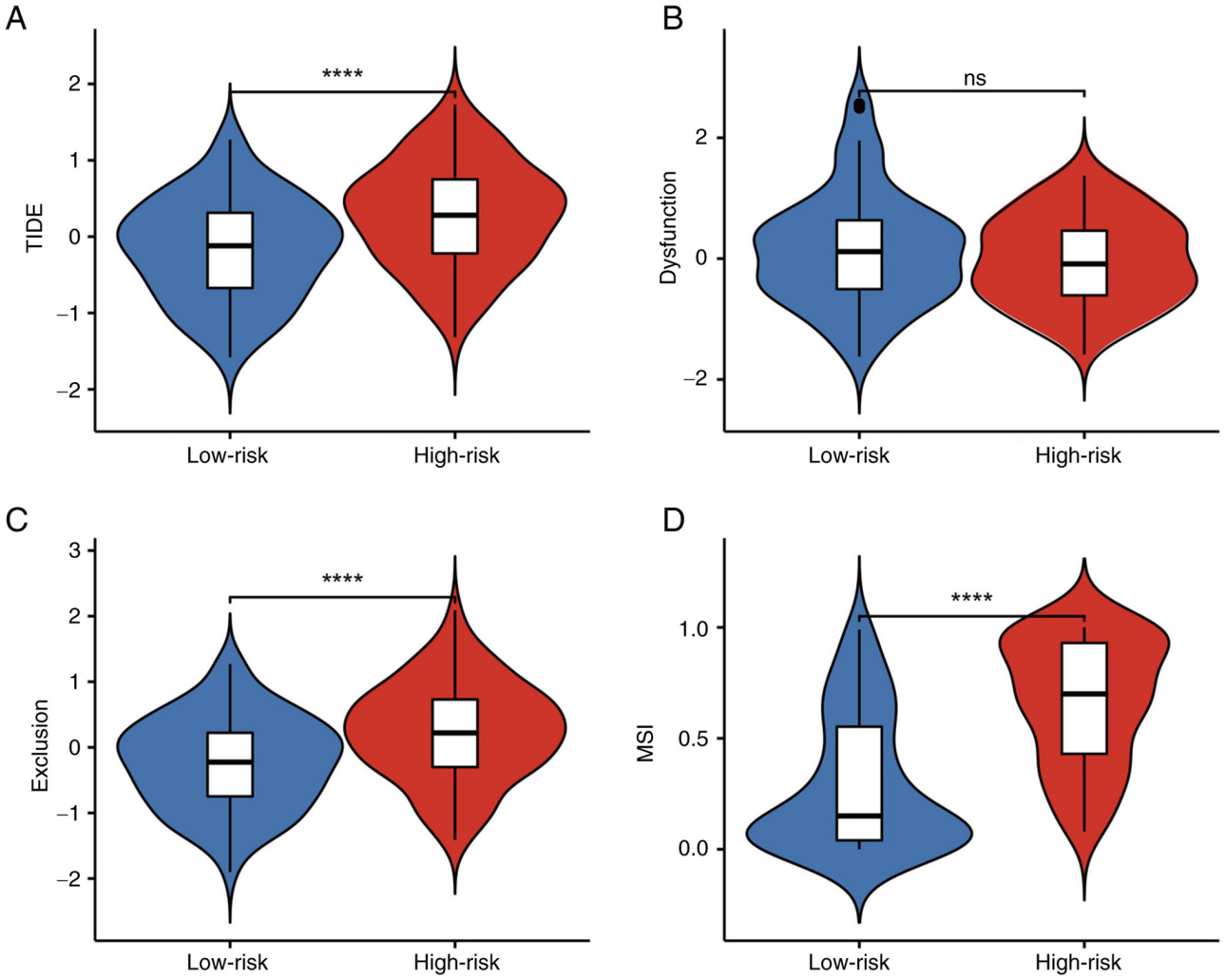

Figure 4. Correlation between DCAF13 expression and TIDE Scores. (A) TIDE score in high- vs. low-DCAF13 expression groups. (B) T-cell dysfunction score in high- vs. low-DCAF13 expression groups. (C) T-cell exclusion score in high- vs. low-DCAF13 expression groups. (D) MSI score in high- vs. low-DCAF13 expression groups ****P<0.0001. ns, not significant; DACF13, DDB1- and CUL4-associated factor 13; MSI, microsatellite instability.

TNM stage (HR=1.398; P<0.05) were independent prognostic factors for poor 5-year OS (Table III). KM survival analysis demonstrated that patients with CRC with high DCAF13 expression had a significantly shorter OS compared with those with low or no DCAF13 expression (Fig. 5B). Furthermore, survival analysis according to TNM stage revealed a clear prognostic stratification, with stage I patients showing the most favourable survival, stage II patients exhibiting intermediate outcomes and stage III/IV patients having the worst prognosis, and the differences among TNM stages were statistically significant (Fig. 5B). Additionally, western blotting analysis demonstrated that, compared with normal colon cells (FHC cells), DCAF13 expression was significantly elevated in CRC cell lines, particularly in RKO cells (Fig. 5C and D).

Effect of DCAF13 knockdown on CRC cells. To confirm the pro-tumorigenic role of DCAF13 on CRC progression, lentivirus-mediated shRNA was used to knock down DCAF13 expression in RKO cells. RT-qPCR results confirmed that DCAF13 expression levels in the shDCAF13 were significantly reduced compared with control cells (Fig. 6A). As confirmed by western blotting analysis, DCAF13 expression levels also showed a similar reduction, validating the knockdown efficacy (Fig. 6B and C). Cell proliferation assays revealed that DCAF13 knockdown significantly impaired the proliferative potential of RKO cells (Fig. 6D). In parallel, the expression of the cell proliferation marker PCNA was significantly decreased in shDCAF13 cells, further confirming the reduction in proliferation (Fig. 6E and F). Migration assays, performed using scratch and Transwell assays, demonstrated that DCAF13 knockdown significantly abrogated the ability of RKO cells to migrate compared with that of the shNC group (Fig. 6G-J). Furthermore, the colony formation and adhesion assays showed significant reductions in the number of colonies and adherent cells following DCAF13 knockdown compared with that of the control group (Fig. 6K-N). Cell cycle distribution analysis revealed that DCAF13 knockdown induced a G_1 phase arrest, indicating a disruption in cell cycle progression (Fig. 6O and P). Corresponding western blotting analysis showed that, compared with shNC cells, knockdown of DCAF13 resulted in increased expression of the epithelial marker E-cadherin and decreased expression of the mesenchymal markers N-cadherin and vimentin in CRC

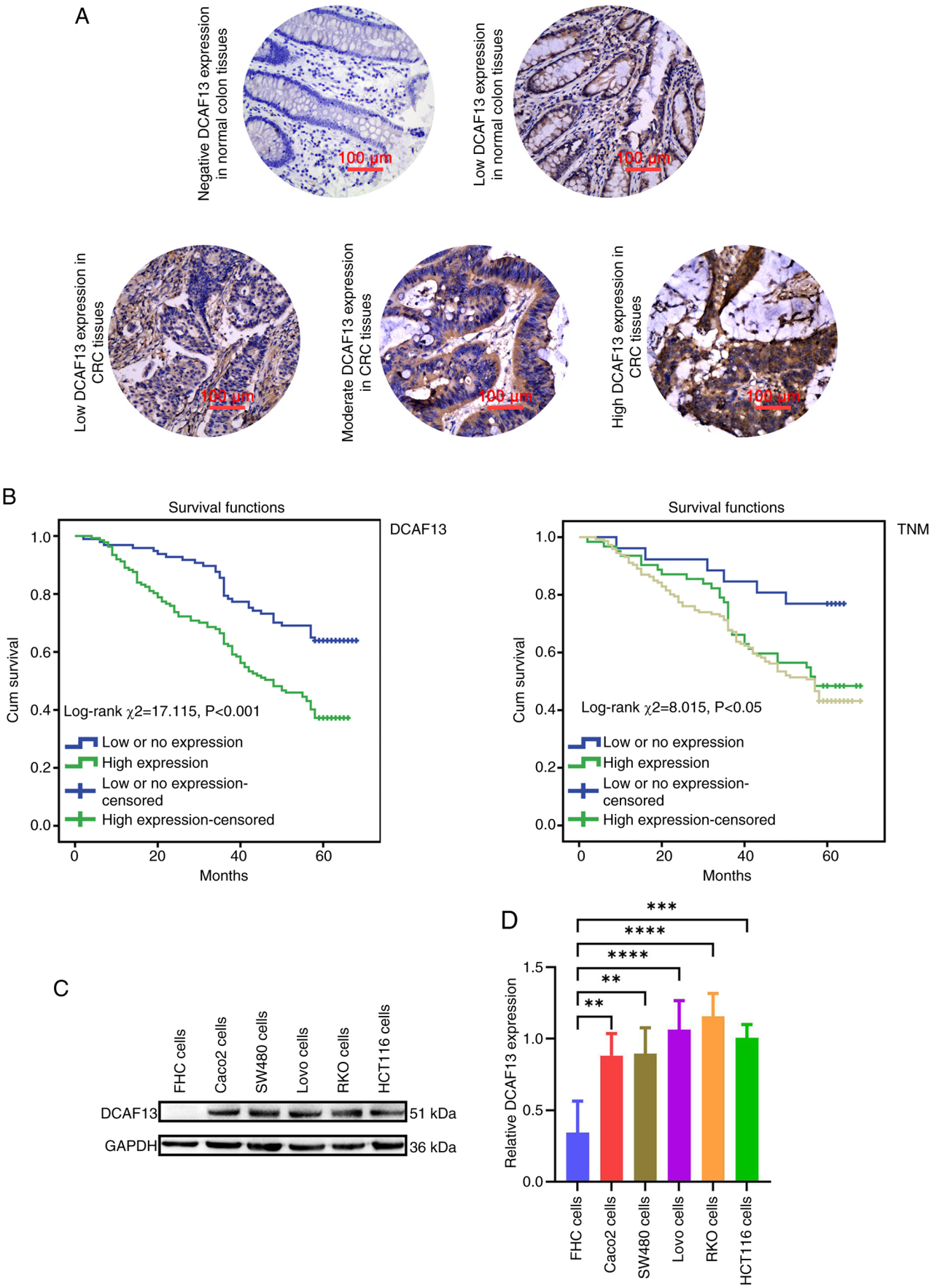

Figure 5. Expression of DCAF13 in CRC tissues/cells and survival analysis of patients with CRC. (A) Representative immunohistochemical staining results of DCAF13 in normal colon and CRC tissues. Scale bar, 100 mm. (B) Overall survival rates in patients with CRC included in the present study. Patients without the event of interest at the last follow-up or lost to follow-up were treated as censored. (C) Representative result of DCAF13 expression levels in normal colon and CRC cells. (D) Relative expression levels of DCAF13 protein expression levels in normal colon and CRC cells. **P<0.01, ***P<0.001 and ****P<0.0001. CRC, colorectal cancer; DACF13, DDB1- and CUL4-associated factor 13; Cum, cumulative.

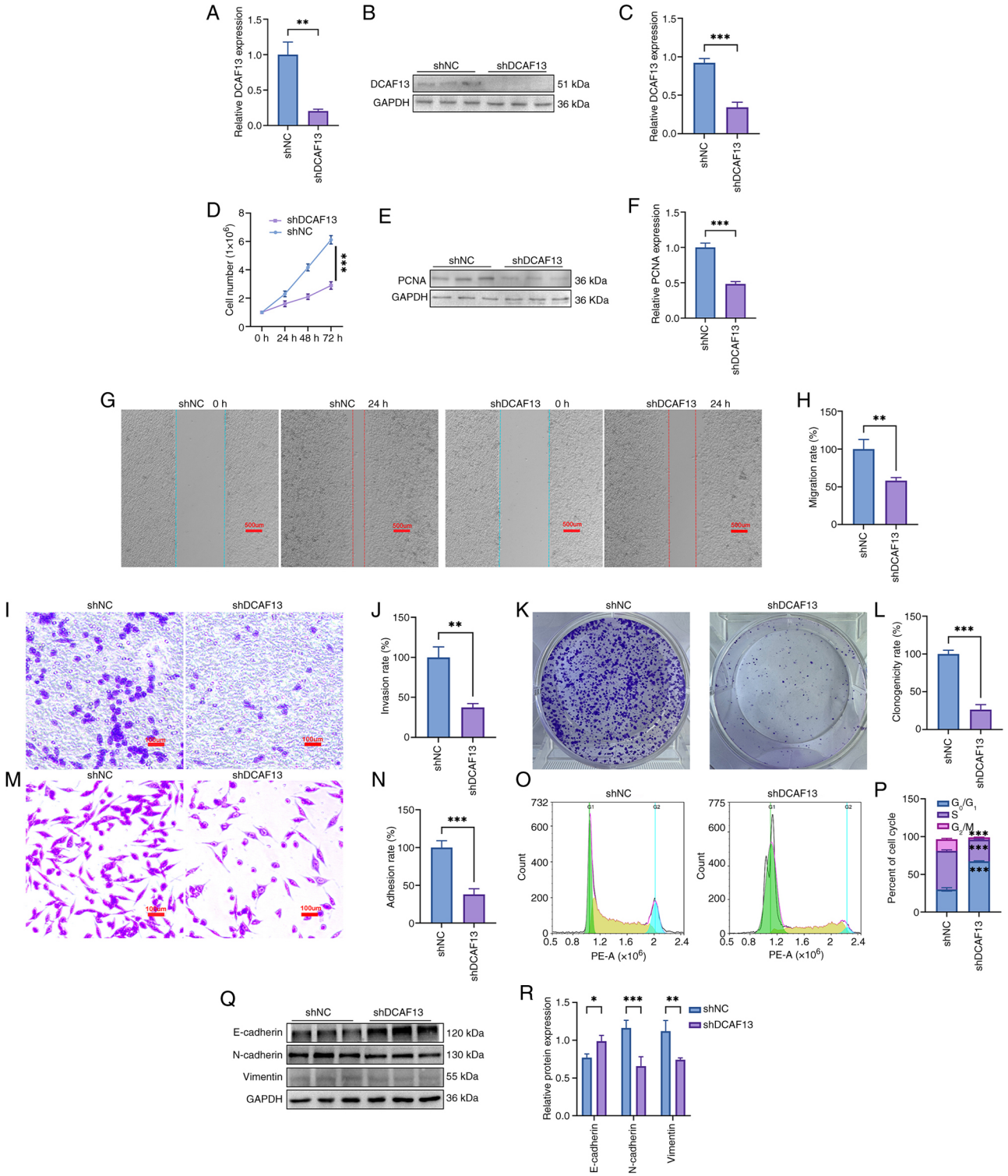

Figure 6. Effects of DCAF13 knockdown on inhibiting the malignant behaviour of RKO cells. (A) Detection of DCAF13 knockdown efficiency using quantitative reverse transcription-quantitative PCR. (B) Detection of DCAF13 knockdown efficiency using western blot. (C) Quantitative DCAF13 expression levels. (D) Cell growth curve. (E) Representative PCNA expression results. (F) Quantitative PCNA expression levels. (G) Representative result of cell migration. Scale bar, 500 μm (H) Quantitative result of cell migration. (I) Representative result of cell migration by Transwell assay. Scale bar, 100 μm. (J) Quantitative result of the cell migration assay by Transwell assay. (K) Representative result of the clonogenicity assay. (L) Quantitative result of clonogenicity assay. (M) Representative result of cell adhesion. Scale bar, 100 μm. (N) Quantitative result of the cell adhesion assay. (O) Cell cycle distribution. (P) Percentage of cells in each cell cycle phase. (Q) Representative expression result of EMT-related proteins. (R) Relative expression levels of ETM-related proteins. *P<0.05, **P<0.01, ***P<0.001. CRC, colorectal cancer; DACF13, DDB1- and CUL4-associated factor 13; PCNA, proliferating cell nuclear antigen; sh, short hairpin; EMT, epithelial-to-mesenchymal transition.

cells (Fig. 6Q and R), further supporting the involvement of DCAF13 in regulating EMT progression in CRC cells.

Effect of DCAF13 knockdown on alterations in the transcriptome of RKO cells. To further uncover the pro-tumourigenic

effect of DCAF13 on CRC progression, the transcriptome characteristics of DCAF13 knockdown RKO cells were analysed. The results confirmed that a total of 12,652 transcripts were mined in the RKO cells between the shNC and shDCAF13 groups. The volcano plot identified 423 DEGs between the shNC and shDCAF13 groups; this comprised 219 upregulated DEGs and 204 downregulated DEGs in the shDCAF13 group when compared with the shNC group (Fig. 7A). A distinct hierarchical clustering of genes in the shDCAF13 RKO cells compared with the shNC group was demonstrated in the heat map (Fig. 7B). Conventionally, the functional GO enrichment analyses were performed to determine the overall functional implications of these identified DEGs. In terms of biological processes (Fig. 7C), the identified DEGs were predominantly involved in the subcategories of 'locomotion', 'growth' and 'biological adhesion'. KEGG pathway enrichment analysis indicated significant involvement of multiple oncogenic and immune-related pathways, such as 'TNF signalling pathway', 'MAPK signalling pathway', 'cytokine-cytokine receptor interaction' and 'NOD-like receptor signalling pathway', which highlighted the potential role of DCAF13 in modulating tumour biology (Fig. 7D). GSEA results further demonstrated the TNF signalling pathway and homologous recombination as central regulatory pathways that potentially mediate the pro-tumourigenic effects of DCAF13 in CRC progression (Fig. 7E and F), which was further validated by the increased expression levels of γ-H2AX and decreased ATM expression levels in the shDCAF13 group when compared with that of the shNC group (Fig. 8). These results suggest an association between DCAF13 depletion and elevated DNA damage signalling.

Discussion

CRC remains a leading cause of cancer-related mortality globally. Advanced stages of CRC are often characterised by metastasis, drug resistance and immune evasion, which severely complicate treatment and contribute to a poor prognosis (47). While traditional therapies, including chemotherapy and surgery, have led to improvements in survival rates, metastatic CRC still poses a major challenge (2). The prognosis for patients with metastatic CRC remains poor, with a median 5-year survival of 12.5% in the USA (48). Recent advances in immunotherapy offer hope, particularly for patients with tumours that are resistant to conventional treatments. The emergence of ICIs, such as pembrolizumab and nivolumab, has marked a breakthrough in CRC treatment (48,49). Approvals from the Food and Drug Administration of ICIs that target the programmed cell death 1 PD-1/PD-L1 and cytotoxic T lymphocyte antigen 4 (CTLA4), have shown significant survival benefits in patients with dMMR or MSI-H CRC, which are characterised by high mutational burdens (50,51). By contrast, patients with proficient mismatch repair (pMMR) tumours, including those with microsatellite stability (MSS) or low-level microsatellite instability (MSI-L), typically exhibit low levels of tumour-infiltrating lymphocytes and show only modest responses to immune checkpoint inhibitors (52,53).

To identify novel biomarkers and therapeutic targets that may enhance the efficacy of immunotherapy, particularly in pMMR/MSS CRC, DCAF13, a substrate receptor within the CUL4-DDB1 E3 ubiquitin ligase complex, was assessed in the present study. This protein complex regulates protein turnover through the ubiquitin-proteasome system and is known to influence processes such as DNA damage repair, cell cycle progression and immune regulation. Recent studies have implicated DCAF13 in tumorigenesis, metastasis and chemoresistance across several malignancies, including breast and ovarian cancer (18,25). These findings prompted further investigation of the expression patterns, clinical relevance and immunological implications of DCAF13 in CRC.

The TME serves a central role in immune evasion in CRC through mechanisms such as the upregulation of immune checkpoints and the presence of immunosuppressive cells (47,54). CRC tumours enriched with tumour-infiltrating lymphocytes and an inflamed TME tend to exhibit improved responses to ICIs (55). Considering these challenges, combination therapies that pair ICIs with chemotherapy, targeted therapies or immune modulators are being actively explored. Personalised immunotherapy, guided by molecular profiles and predictive biomarkers such as PD-L1 expression, MSI status and tumour mutational burden (TMB) holds notable potential (56-58). Despite these advances, the clinical challenges remain, particularly the heterogeneous nature of CRC. In addition, current ICIs are largely ineffective in patients with pMMR and MSS or MSI-L tumours (48). Low TMB and a lack of immune cell infiltration in these tumours are considered key mechanisms of immune resistance (48). Ongoing research into combination strategies, TME modulation and the identification of novel immunotherapy biomarkers will be critical for optimising immunotherapeutic outcomes in CRC.

DCAFs regulates the ubiquitin-proteasome system (UPS) to maintain cellular homeostasis (59). The UPS governs the degradation of proteins involved in critical cellular functions, including DNA repair, transcription, cell cycle regulation and apoptosis. DCAFs are essential for substrate recognition and specificity within the UPS, making them integral to maintaining cellular functions that, when disrupted, may contribute to cancer progression (60). An increasing body of research into DCAF proteins has revealed their involvement in tumorigenesis, metastasis, immune evasion and chemoresistance, highlighting their potential as therapeutic targets (61,62). DCAF1 (also known as VprBP) and DCAF2 (also known as CDT2), for example, are key regulators of DNA damage repair and cell cycle progression, processes that are key to cancer development (63,64). Additionally, DCAF proteins, particularly DCAF13, have been implicated in chemotherapy resistance through their role in the CUL4-DDB1 E3 ubiquitin ligase complex, which targets key regulatory proteins for polyubiquitination and proteasomal degradation. Although direct modulation of classical drug-metabolising enzymes by DCAF13 has not been demonstrated, recent studies have shown that DCAF13 negatively regulates the stability of tumour suppressors such as PTEN and epigenetic enzymes such as SUV39H1. Furthermore, in breast cancer, DCAF13 has been identified as an RNA-binding protein that promotes the degradation of *DTX3* mRNA (21,23,27). Notably, doxorubicin treatment was found to upregulate DCAF13 expression levels, thereby enhancing cancer cell migration, and EMT, suggesting a potential mechanism by which chemotherapy may inadvertently promote metastasis in drug-resistant tumours (65).

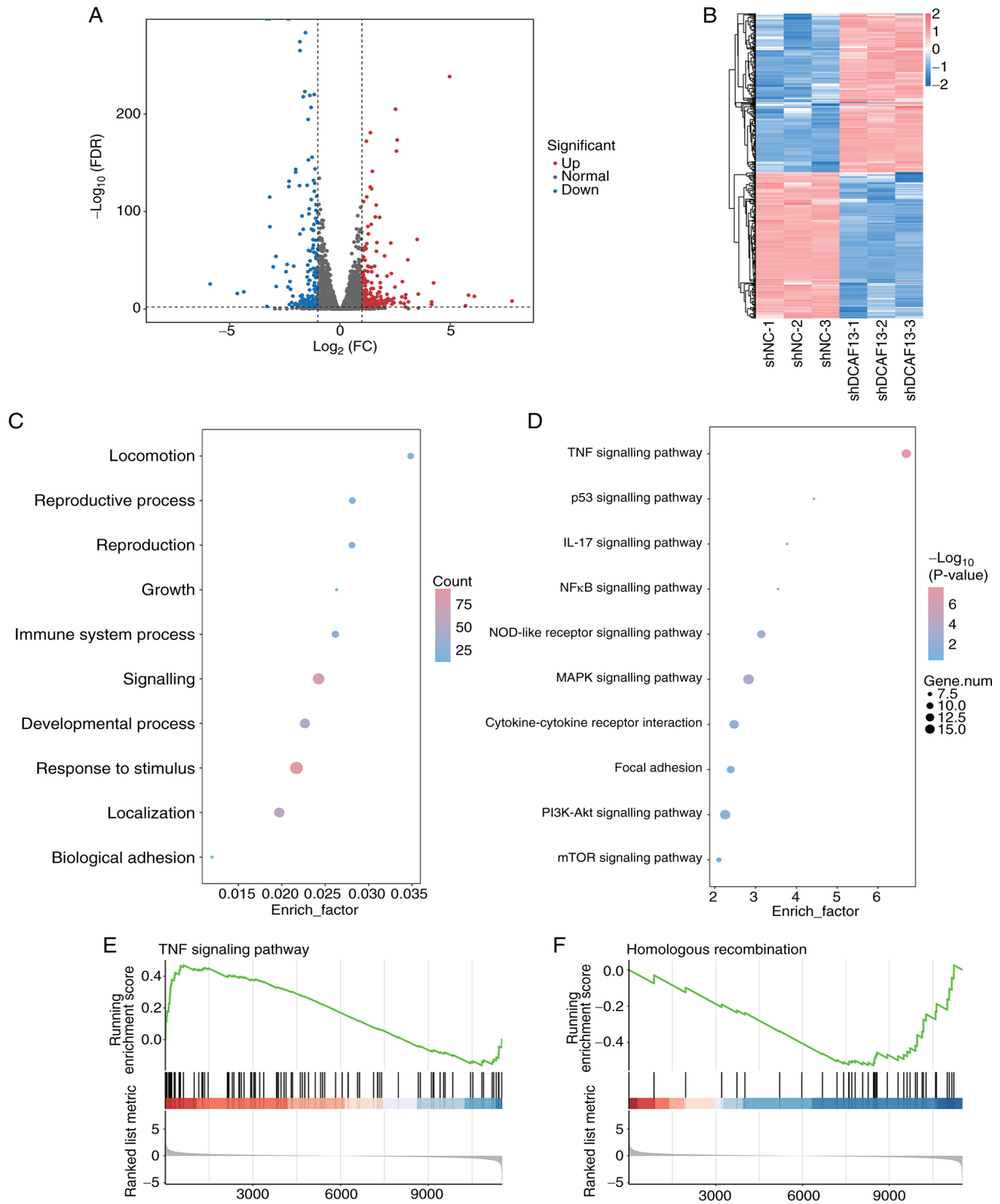

Figure 7. Effects of DCAF13 knockdown on triggering transcriptome alterations of RKO cells. (A) Volcano plots of DEGs. (B) Heat map of DEGs. (C) Biological process of GO enrichment analysis. (D) KEGG pathway enrichment analysis. (E) TNF signalling pathway enriched based on KEGG of GSEA. (F) Homologous recombination enriched based on KEGG of GSEA. DACF13, DDB1- and CUL4-associated factor 13; GO. Gene Ontology; KEGG, Kyoto Encyclopaedia of Genes and Genomes; GSEA, Gene Set Enrichment Analysis; FC, fold change; FDR, false discovery rate.

These findings have prompted growing interest in targeting DCAF13 to overcome resistance to therapy.

A previous study has further emphasised the role of DCAF proteins in CRC, particularly DCAF4L2, which is upregulated in

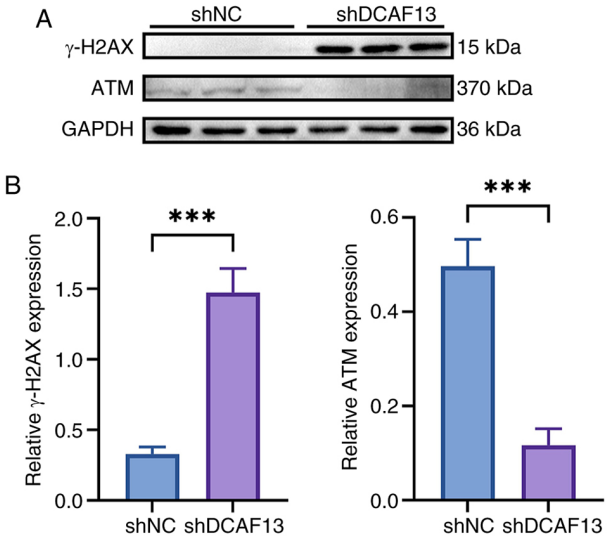

Figure 8. Effects of DCAF13 knockdown the expression of homologous recombination-related proteins in RKO cells. (A) Representative expression of homologous recombination-related proteins. (B) Relative expression levels of homologous recombination-related proteins. ***P<0.001. DACF13, DDB1- and CUL4-associated factor 13.

CRC cell lines and patient tissues (66). Upregulated expression of DCAF4L2 in CRC is associated with enhanced cell migration and metastatic potential, suggesting its involvement in tumour initiation and progression. By modulating the CUL4A-DDB1 complex, DCAF proteins regulate critical cellular processes such as cell cycle control and DNA repair, reinforcing their involvement in CRC pathogenesis. In addition, targeting the DCAF-CUL4A-DDB1 interaction with small-molecule inhibitors such as NSC1892 has shown promise in preclinical models, suppressing CRC cell proliferation and migration (67). Furthermore, the integration of DCAF-related pathways with immune checkpoint regulation and TME modulation highlights novel possibilities for enhancing immunotherapy efficacy (68). As such, DCAF proteins represent a promising molecular target in CRC, and ongoing research into their mechanistic roles and therapeutic potential is crucial. Their modulation could offer novel avenues for precision medicine in CRC, improving treatment strategies and patient outcomes.

In the present study, it was shown that DCAF13 expression was upregulated in various solid tumours, including CRC. Specifically, CRC tissues exhibited higher levels of DCAF13 compared with that of adjacent normal tissues. This finding is consistent with previous studies, such as that of Ieranò *et al* (69), who reported elevated DCAF13 protein expression levels in CRC tissues relative to adjacent normal samples. The results of the present study, further confirmed by the results of analysis of data obtained from TCGA and the GSE40967 cohorts, as well as by the IHC staining of clinical CRC samples, corroborate these findings. Furthermore, KM survival analysis demonstrated that higher expression of DCAF13 was associated with a shorter OS in patients with CRC, suggesting that DCAF13 may serve as a prognostic biomarker. External validation with independent cohorts and IHC staining experiments of the clinical samples confirmed the robustness and reliability of this marker, further supporting its potential as a therapeutic target.

According to a previous study, high DCAF13 expression is associated with an immunosuppressive TME and resistance to immunotherapy (27). Correspondingly, in the present study, analysis of the immune microenvironment demonstrated the correlation between DCAF13 expression and TIICs, as well as immune checkpoint molecules. As TIICs are known to serve significant prognostic and therapeutic roles in CRC and other types of cancer (70,71), this finding is particularly relevant. The present study also demonstrated that high DCAF13 expression was associated with increased responsiveness to immune checkpoint blockade therapy, as indicated by immune checkpoint analysis and TIDE scores. TIDE is a computational framework designed to model tumour immune evasion mechanisms and to predict patient response to ICIs, such as anti-programmed cell death 1 (PD-1)/programmed cell death 1 ligand (PD-L1) therapies. Specifically, TIDE evaluates two major mechanisms of immune escape. The first is T cell dysfunction, which occurs in tumours with high levels of cytotoxic T lymphocyte (CTL) infiltration. In such cases, although CTLs are present in the TME, their antitumour activity is impaired due to exhaustion or other suppressive mechanisms. The second mechanism is T cell exclusion, where CTLs fail to infiltrate the tumour, often due to barriers in the TME or immunosuppressive signalling pathways that prevent effective T cell trafficking. In addition to these two components, TIDE also incorporates an MSI score, which reflects the degree of dMMR in tumour cells (72,73). High MSI levels are typically associated with increased neoantigen load and an improved response to ICIs. These findings suggest that DCAF13 may serve as a valuable predictor of immunotherapy efficacy in CRC. Nevertheless, further mechanistic studies are required to clarify how DCAF13 modulates TIICs and immune checkpoint interactions.

The analysis performed in the present study also identified significant differences in SSs among patients with CRC, in agreement with prior research highlighting the contribution of stromal components to tumour progression, metastasis and resistance to therapy (74,75). A significant difference in the ISs among patients with CRC was also observed, which is likely attributed to variations in the proportions of immune cell populations. These results suggested that DCAF13 expression may influence CRC progression and metastasis by modulating the immune microenvironment. Additionally, DCAF13 expression was positively correlated with immune cell populations such as M0 and M1 macrophages, activated mast cells, neutrophils and $CD4^+$ memory T cells in CRC, further highlighting the potential application of targeting DCAF13 for improving the efficacy of immunotherapy in patients with CRC.

Consistent with the results of Shan *et al* (18), the present study demonstrated that the knockdown of DCAF13 significantly suppressed proliferation, colony formation, migration and adhesion in CRC cells, as well as disturbing cell cycle progression, EMT and transcriptome characteristics of CRC cells. These phenotypic changes further supported the results of CancerSEA analysis, which indicated the pro-tumourigenic role of DCAF13 in promoting the proliferation, migration, clonogenicity, adhesion, metastasis and EMT progression of CRC cells.

Mechanistically, the KEGG pathway and GSEA results in the present study underscored the pivotal role of homologous

recombination and the 'TNF signalling pathway' as key regulatory mechanisms mediating the pro-tumourigenic effects of DCAF13 in CRC progression. Homologous recombination, a highly regulated DNA repair mechanism essential for maintaining genomic integrity in response to DNA double-stranded breaks (DSBs) or lesions, protects cells from exogenous and endogenous DNA damage (76). The homologous recombination deficiency (HRD) and homologous recombination repair pathway gene mutations, comprising at least 10 key genes (*ATM*, *BARD1*, *BRCA1*, *BRCA2*, *BRIP1*, *CHEK2*, *NBS1(NBN)*, *PALB2*, *RAD51C* and *RAD51D*), are frequently associated with inherited susceptibility to several types of cancer, including breast, ovarian, prostate and pancreatic cancer (77,78). As a well-recognised characteristic of tumours, HRD induces the activation of error-prone DNA damage repair mechanisms, which, while attempting to repair DNA, often result in the accumulation of DSBs, promoting genomic instability and eventual cell death (79). Additionally, HRD also enhances cellular sensitivity to DNA-targeted therapies, including platinum-based chemotherapy, DSB-inducing agents and poly (ADP-ribose) polymerase (PARP) inhibitors (80,81). Notably, accumulating evidence has revealed that tumours with HRD often exhibit a high mutational load, resulting in increased levels of TMB, tumour neoantigen burden and neoantigen expression, which may increase tumour-cell recognition by T cells, thus facilitating an effective lymphoid immune response and potentially improving prognosis and survival outcomes (82,83). Notably, Liu *et al* (84) demonstrated that HRD suppressed TNF-α expression via the JNK/c-Jun signalling pathway in triple-negative breast cancer cells and patient tissues, thereby negatively regulating PD-L1 expression. This suggests a role for HRD in modulating immune responses, further supporting the potential of HRD testing for cancer diagnosis and treatment via immune regulation.

In the present study, knockdown of *DCAF13* impaired the homologous recombination process, as indicated by changes in the expression levels of key homologous recombination markers, including ATM and γ-H2AX, in RKO cells. These findings align with previous research showing that DCAF8L2 overexpression disrupts homologous recombination in breast cancer cells by promoting the ubiquitination and degradation of BARD1, thereby increasing sensitivity to DNA damage and facilitating cancer progression (85). Given the critical role of DCAF13 in homologous recombination, it could be suggested that its dysregulation may affect tumour sensitivity to DNA-damaging agents, such as platinum-based chemotherapeutics and PARP inhibitors. Notably, multi-omics approaches, particularly those integrating genomics and pharmacogenomics, have demonstrated strong predictive power in assessing drug responses and identifying synergistic targets (86,87). Future studies should incorporate these approaches to comprehensively evaluate the correlation between DCAF13 expression and sensitivity to DNA-damaging agents. Furthermore, considering the established interplay between DNA repair defects and immunogenicity, combining DCAF13 inhibition with immune checkpoint blockade (such as anti-PD-1/PD-L1 or CTLA-4 therapies) may yield synergistic effects. This combination strategy is especially promising for immunologically 'cold' CRC tumours, which are often refractory to conventional ICIs (88). These insights support the rationale for exploring DCAF13 as a dual-function biomarker and therapeutic target in precision oncology (27,69).

Several limitations of the present study should be acknowledged. Notably, the absence of single-cell RNA sequencing (scRNA-seq) and spatial transcriptomics data restricts the resolution of the analysis regarding the heterogeneity and spatial architecture of the tumour immune microenvironment. These cutting-edge multi-omics techniques, especially when combined with transcriptomic, proteomic and metabolomic layers, are increasingly regarded as essential tools for elucidating tumour heterogeneity, identifying drug resistance pathways and optimising immunotherapy strategies (86,87). By integrating scRNA-seq and spatial transcriptomic technologies, future research will more accurately map the immune cell subtypes and their spatial distributions in tumours with high DCAF13 expression, thereby providing direct evidence for the immunomodulatory role of DCAF13 and facilitating the development of precision immunotherapies.

In conclusion, the present study demonstrated that DCAF13 is aberrantly upregulated in CRC and is closely associated with CRC progression. Through comprehensive cellular analyses, it was demonstrated that DCAF13 served a pivotal role in regulating key cellular processes such as proliferation, migration, metastasis, EMT and homologous recombination in CRC. These findings provide novel insights into the pro-tumourigenic functions of DCAF13, underscoring its potential as a critical regulator in CRC pathophysiology. However, further investigations are required to fully elucidate the precise molecular mechanisms through which DCAF13 modulates homologous recombination and its impact on therapeutic responses. Specifically, understanding how DCAF13 influences DNA repair pathways and immune regulation could offer novel avenues for improving the effectiveness of DNA-targeted therapies and ICIs in CRC treatment in the future.

Acknowledgements

Not applicable.

Funding

The present study was supported by the Natural Science Foundation of Inner Mongolia (grant no. 2025MS08125), the National Natural Science Foundation of China (grant nos. 82060567 and 82360551), Outstanding Young Talents Cultivation Program of Grassland Elite in Inner Mongolia (grant no. Q202286), Zhiyuan Talents Cultivation Program of Mongolia Medical University (grant no. ZY20242129), Inner Mongolia Medical University Affiliated Hospital Talent Training Project-Sailing Series, the Health Science and Technology Project of Chu Zhou (grant no. 2022003) and the Public Hospital Scientific Research Joint Fund Project (grant no. 2025NMWJKJXM1167).

Availability of data and materials

The data generated in the present study may be found in the Genome Sequence Archive in National Genomics Data Center, China National Center for Bioinformation/Beijing Institute

of Genomics, Chinese Academy of Sciences database under accession number GSA-Human: HRA012999, which is associated with BioProject PRJCA045205 or at the following URLs: https://ngdc.cncb.ac.cn/bioproject/browse/PRJCA045205 and https://ngdc.cncb.ac.cn/gsa-human/browse/HRA012999. The other data generated in the present study may be requested from the corresponding author.

Authors' contributions

WZ, LS and GL performed study conceptualization. WZ, RZ, MJ, SL, FL, QJ and GL developed the methodology. WZ, RZ, MJ and SL performed data validation. WZ, MJ and FL performed bioinformatics data processing and analysis. RZ, MJ and SL conducted the cell biology and molecular biology experiments. QJ was responsible for clinical sample collection, immunohistochemical staining, and patient prognostic analysis. WZ, RZ, MJ and GL performed formal data analysis. WZ, LS and GL acquired funding. LS and GL provided resources and supervision. GL wrote the manuscript. WZ and GL confirm the authenticity of all the raw data. All authors read and approved the final version of the manuscript.

Ethics approval and consent to participate

The present study was approved by the Ethical Review Committee of Inner Mongolia Medical University (approval no. 2022513411; Hohhot, China) and was performed in accordance with the Declaration of Helsinki. Informed consent was written from all patients prior to inclusion in the study.

Patient consent for publication

Not applicable.

Competing interests

The authors declare that they have no competing interests.

References

1. Eng C, Yoshino T, Ruíz-García E, Mostafa N, Cann CG, O'Brian B, Benny A, Perez RO and Cremolini C: Colorectal cancer. Lancet 404: 294-310, 2024.
2. Biller LH and Schrag D: Diagnosis and treatment of metastatic colorectal cancer: A Review. JAMA 325: 669-685, 2021.
3. Uneyama M, Chambers JK, Nakashima K, Uchida K and Nakayama H: Histological classification and immunohistochemical study of feline colorectal epithelial tumors. Vet Pathol 58: 305-314, 2021.
4. Marusyk A, Janiszewska M and Polyak K: Intratumor heterogeneity: The Rosetta Stone of therapy resistance. Cancer Cell 37: 471-484, 2020.
5. GBD 2019 Colorectal Cancer Collaborators: Global, regional, and national burden of colorectal cancer and its risk factors, 1990-2019: A systematic analysis for the global burden of disease study 2019. Lancet Gastroenterol Hepatol 7: 627-647, 2022.
6. Zygulska AL and Pierzchalski P: Novel diagnostic biomarkers in colorectal cancer. Int J Mol Sci 23: 852, 2022.
7. Gerstberger S, Jiang Q and Ganesh K: Metastasis. Cell 186: 1564-1579, 2023.
8. Arnold M, Sierra MS, Laversanne M, Soerjomataram I, Jemal A and Bray F: Global patterns and trends in colorectal cancer incidence and mortality. Gut 66: 683-691, 2017.
9. Dekker E, Tanis PJ, Vleugels JLA, Kasi PM and Wallace MB: Colorectal cancer. Lancet 394: 1467-1480, 2019.
10. Van Cutsem E, Cervantes A, Adam R, Sobrero A, Van Krieken JH, Aderka D, Aranda Aguilar E, Bardelli A, Benson A, Bodoky G, *et al*: ESMO consensus guidelines for the management of patients with metastatic colorectal cancer. Ann Oncol 27: 1386-1422, 2016.
11. Rui R, Zhou L and He S: Cancer immunotherapies: advances and bottlenecks. Front Immunol 14: 1212476, 2023.
12. Naimi A, Mohammed RN, Raji A, Chupradit S, Yumashev AV, Suksatan W, Shalaby MN, Thangavelu L, Kamrava S, Shomali N, *et al*: Tumor immunotherapies by immune checkpoint inhibitors (ICIs); the pros and cons. Cell Commun Signal 20: 44, 2022.
13. Le DT, Durham JN, Smith KN, Wang H, Bartlett BR, Aulakh LK, Lu S, Kemberling H, Wilt C, Luber BS, *et al*: Mismatch repair deficiency predicts response of solid tumors to PD-1 blockade. Science 357: 409-413, 2017.
14. Yin Q, Wu L, Han L, Zheng X, Tong R, Li L, Bai L and Bian Y: Immune-related adverse events of immune checkpoint inhibitors: A review. Front Immunol 14: 1167975, 2023.
15. Xiao C, Xiong W, Xu Y, Zou J, Zeng Y, Liu J, Peng Y, Hu C and Wu F: Immunometabolism: A new dimension in immunotherapy resistance. Front Med 17: 585-616, 2023.
16. Kawashima S and Togashi Y: Resistance to immune checkpoint inhibitors and the tumor microenvironment. Exp Dermatol 32: 240-249, 2023.
17. Lee J and Zhou P: DCAFs, the missing link of the CUL4-DDB1 ubiquitin ligase. Mol Cell 26: 775-780, 2007.
18. Shan BQ, Wang XM, Zheng L, Han Y, Gao J, Lv MD, Zhang Y, Liu YX, Zhang H, Chen HS, *et al*: DCAF13 promotes breast cancer cell proliferation by ubiquitin inhibiting PERP expression. Cancer Sci 113: 1587-1600, 2022.
19. Yan X, Rong M, Zhou Q and Zhang C: DCAF13 is essential for the pathogenesis of preeclampsia through its involvement in endometrial decidualization. Mol Cell Endocrinol 556: 111741, 2022.
20. Zhang YL, Zhao LW, Zhang J, Le R, Ji SY, Chen C, Gao Y, Li D, Gao S and Fan HY: DCAF13 promotes pluripotency by negatively regulating SUV39H1 stability during early embryonic development. EMBO J 37: e98981, 2018.
21. Liu J, Li H, Mao A, Lu J, Liu W, Qie J and Pan G: DCAF13 promotes triple-negative breast cancer metastasis by mediating DTX3 mRNA degradation. Cell Cycle 19: 3622-3631, 2020.
22. Wang K, Li L, Fu L, Yuan Y, Dai H, Zhu T, Zhou Y and Yuan F: Integrated bioinformatics analysis the function of RNA binding proteins (RBPs) and their prognostic value in breast cancer. Front Pharmacol 10: 140, 2019.
23. Wei S, Xing J, Chen J, Chen L, Lv J, Chen X, Li T, Yu T, Wang H, Wang K and Yu W: DCAF13 inhibits the p53 signaling pathway by promoting p53 ubiquitination modification in lung adenocarcinoma. J Exp Clin Cancer Res 43: 3, 2024.
24. Zhang WJ, Hu CL, Guo BL, Liang XP, Wang CY and Yang T: STAT5B suppresses ferroptosis by promoting DCAF13 transcription to regulate p53/xCT pathway to promote mantle cell lymphoma progression. Biologics 18: 181-193, 2024.
25. Tang ZY, Wang XM, Xu CW, Sun QQ, Hua YX, Zhou QY, Hu HY, Liu SB, Guo YJ, Ao L, *et al*: DCAF13 promotes ovarian cancer progression by activating FRAS1-mediated FAK signaling pathway. Cell Mol Life Sci 81: 421, 2024.
26. Liu ZY, Li YH, Zhang QK, Li BW and Xin L: Development and validation of a ubiquitin-proteasome system gene signature for prognostic prediction and immune microenvironment evaluation in hepatocellular carcinoma. J Cancer Res Clin Oncol 149: 13363-13382, 2023.
27. Wei S, Lu K, Xing J and Yu W: A multidimensional pan-cancer analysis of DCAF13 and its protumorigenic effect in lung adenocarcinoma. FASEB J 37: e22849, 2023.
28. Zhou L, Wang S, Hu W, Liu X, Xu L, Tong B, Zhang T, Xue Z, Guo Y, Zhao J, *et al*: T cell proliferation requires ribosomal maturation in nucleolar condensates dependent on DCAF13. J Cell Biol 222: e202201096, 2023.
29. Sun Y, Baechler SA, Zhang X, Kumar S, Factor VM, Arakawa Y, Chau CH, Okamoto K, Parikh A, Walker B, *et al*: Targeting neddylation sensitizes colorectal cancer to topoisomerase I inhibitors by inactivating the DCAF13-CRL4 ubiquitin ligase complex. Nat Commun 14: 3762, 2023.
30. Marisa L, de Reyniès A, Duval A, Selves J, Gaub MP, Vescovo L, Etienne-Grimaldi MC, Schiappa R, Guenot D, Ayadi M, *et al*: Gene expression classification of colon cancer into molecular subtypes: Characterization, validation, and prognostic value. PLoS Med 10: e1001453, 2013.

31. Ritchie ME, Phipson B, Wu D, Hu Y, Law CW, Shi W and Smyth GK: limma powers differential expression analyses for RNA-sequencing and microarray studies. Nucleic Acids Res 43: e47, 2015.
32. Yuan H, Yan M, Zhang G, Liu W, Deng C, Liao G, Xu L, Luo T, Yan H, Long Z, *et al*: CancerSEA: A cancer single-cell state atlas. Nucleic Acids Res 47(D1): D900-D908, 2019.
33. Li D, Zhao W, Zhang X, Lv H, Li C and Sun L: NEFM DNA methylation correlates with immune infiltration and survival in breast cancer. Clin Epigenetics 13: 112, 2021.
34. Xiang S, Li J, Shen J, Zhao Y, Wu X, Li M, Yang X, Kaboli PJ, Du F, Zheng Y, *et al*: Identification of prognostic genes in the tumor microenvironment of hepatocellular carcinoma. Front Immunol 12: 653836, 2021.
35. Yang S, Wen L, Chai X, Song Y, Chen X, Chen ZF, Li R, Dong C, Qi Z and Cai Z: The protective effects of taurine and fish oil supplementation on PM2.5-induced heart dysfunction among aged mice: A random double-blind study. Sci Total Environ 851 (Pt 1): 157966, 2022.
36. Tang Z, Li C, Kang B, Gao G, Li C and Zhang Z: GEPIA: A web server for cancer and normal gene expression profiling and interactive analyses. Nucleic Acids Res 45(W1): W98-W102, 2017.
37. Zhang W, Xie M, Huang Q, Liu H, Liu J, Sun X and Li C: STEAP3 is a potential preliminary prognostic biomarker of glioblastoma. Sci Rep 14: 30994, 2024.
38. Xia Y, Zhang R, Wang M, Li J, Dong J, He K, Guo T, Ju X, Ru J, Zhang S and Sun Y: Development and validation of a necroptosis-related gene prognostic score to predict prognosis and efficiency of immunotherapy in gastric cancer. Front Immunol 13: 977338, 2022.
39. Nagtegaal ID, Odze RD, Klimstra D, Paradis V, Rugge M, Schirmacher P, Washington KM, Carneiro F and Cree IA; WHO Classification of Tumours Editorial Board: The 2019 WHO classification of tumours of the digestive system. Histopathology 76: 182-188, 2020.
40. Weiser MR: AJCC 8th Edition: Colorectal cancer. Ann Surg Oncol 25: 1454-1455, 2018.
41. Jin Q, Liu G, Bao L, Ma Y, Qi H, Yun Z, Dai Y and Zhang S: High Spy1 expression predicts poor prognosis in colorectal cancer. Cancer Manag Res 10: 2757-2765, 2018.
42. Wang M, Lan S, Song M, Zhang R, Zhang W, Sun X and Liu G: Synthesis of zinc oxide-doped carbon dots for treatment of triple-negative breast cancer. Int J Nanomed 19: 13949-13971, 2024.
43. Zhang R, Lan S, Jia M, Liu F, Wang M, Jin Q, Su L and Liu G: Theranostic applications of taurine-derived carbon dots in colorectal cancer: Ferroptosis induction and multifaceted antitumor mechanisms. Int J Nanomedicine 20: 7613-7635, 2025.
44. Liu G, Li S, Yuan H, Hao M, Wurihan, Yun Z, Zhao J, Ma Y and Dai Y: Effect of sodium alginate on mouse ovary vitrification. Theriogenology 113: 78-84, 2018.
45. Wang M, Lan S, Zhang W, Jin Q, Du H, Sun X, He L, Meng X, Su L and Liu G: Anti-Cancer potency of copper-doped carbon quantum dots against breast cancer progression. Int J Nanomed 19: 1985-2004, 2024.
46. Zhang W, Sun J, Liu F, Li S, Wang X, Su L and Liu G: Alleviative effect of lactoferrin interventions against the hepatotoxicity induced by titanium dioxide nanoparticles. Biol Trace Elem Res 202: 624-642, 2023.
47. Shin AE, Giancotti FG and Rustgi AK: Metastatic colorectal cancer: Mechanisms and emerging therapeutics. Trends Pharmacol Sci 44: 222-236, 2023.
48. Ganesh K, Stadler ZK, Cercek A, Mendelsohn RB, Shia J, Segal NH and Diaz LA Jr: Immunotherapy in colorectal cancer: Rationale, challenges and potential. Nat Rev Gastroenterol Hepatol 16: 361-375, 2019.
49. Fan A, Wang B, Wang X, Nie Y, Fan D, Zhao X and Lu Y: Immunotherapy in colorectal cancer: Current achievements and future perspective. Int J Biol Sci 17: 3837-3849, 2021.
50. Kasi PM, Budde G, Krainock M, Aushev VN, Koyen Malashevich A, Malhotra M, Olshan P, Billings PR and Aleshin A: Circulating tumor DNA (ctDNA) serial analysis during progression on PD-1 blockade and later CTLA-4 rescue in patients with mismatch repair deficient metastatic colorectal cancer. J Immunother Cancer 10: e003312, 2022.
51. Salewski I, Kuntoff S, Kuemmel A, Feldtmann R, Felix SB, Henze L, Junghanss C and Maletzki C: Combined vaccine-immune-checkpoint inhibition constitutes a promising strategy for treatment of dMMR tumors. Cancer Immunol Immunother 70: 3405-3419, 2021.
52. Le DT, Uram JN, Wang H, Bartlett BR, Kemberling H, Eyring AD, Skora AD, Luber BS, Azad NS, Laheru D, *et al*: PD-1 blockade in tumors with mismatch-repair deficiency. N Engl J Med 372: 2509-2520, 2015.
53. Wang W, Mei Z, Chen Y, Jiang J, Qu Y, Saifuding K, Zhou N, Bulibu G, Tang Y, Zhai X and Jiang Z: Immune checkpoint inhibitors for patients with mismatch repair deficient or microsatellite instability-high advanced cancers: A meta-analysis of phase I-III clinical trials. Int J Surg 111: 1357-1372, 2025.
54. Kazama K, Otake J, Satoyoshi T, Shiozawa M, Sugano N, Sato S, Atsumi Y, Kano K, Murakawa M, Maezawa Y, *et al*: Distribution of regulatory T-cells and other phenotypes of T-cells in tumors and regional lymph nodes of colorectal cancer patients. In Vivo 34: 849-856, 2020.
55. Bai Z, Zhou Y, Ye Z, Xiong J, Lan H and Wang F: Tumor-Infiltrating lymphocytes in colorectal cancer: the fundamental indication and application on immunotherapy. Front Immunol 12: 808964, 2021.
56. Yamaguchi H, Hsu JM, Sun L, Wang SC and Hung MC: Advances and prospects of biomarkers for immune checkpoint inhibitors. Cell Rep Med 5: 101621, 2024.
57. Wang C, Wang HN and Wang L: Biomarkers for predicting the efficacy of immune checkpoint inhibitors. J Cancer 13: 481-495, 2022.
58. Mc Neil V and Lee SW: Advancing cancer treatment: A review of immune checkpoint inhibitors and combination strategies. Cancers (Basel) 17: 1408, 2025.
59. Stier A, Gilberto S, Mohamed WI, Royall LN, Helenius J, Mikicic I, Sajic T, Beli P, Müller DJ, Jessberger S and Peter M: The CUL4B-based E3 ubiquitin ligase regulates mitosis and brain development by recruiting phospho-specific DCAFs. EMBO J 42: e112847, 2023.
60. Jang SM, Redon CE and Aladjem MI: Switching DCAFs: Beyond substrate receptors. BioEssays 43: e2100057, 2021.
61. Zhou Z, Song X, Wavelet CM and Wan Y: Cullin 4-DCAF proteins in tumorigenesis. Adv Exp Med Biol 1217: 241-259, 2020.
62. Miao Q, Kadam VD, Mukherjee A, Tan Z and Teng M: Unlocking DCAFs To catalyze degrader development: An arena for innovative approaches. J Med Chem 66: 13369-13383, 2023.
63. Pan WW, Zhou JJ, Yu C, Xu Y, Guo LJ, Zhang HY, Zhou D, Song FZ and Fan HY: Ubiquitin E3 ligase CRL4(CDT2/DCAF2) as a potential chemotherapeutic target for ovarian surface epithelial cancer. J Biol Chem 288: 29680-29691, 2013.
64. Ghate NB, Kim S, Mehmood R, Shin Y, Kim K and An W: VprBP/DCAF1 regulates p53 function and stability through site-specific phosphorylation. Oncogene 42: 1405-1416, 2023.
65. Sun Z, Zhou D, Yang J and Zhang D: Doxorubicin promotes breast cancer cell migration and invasion via DCAF13. FEBS Open Bio 12: 221-230, 2022.
66. Wang H, Chen Y, Han J, Meng Q, Xi Q, Wu G and Zhang B: DCAF4L2 promotes colorectal cancer invasion and metastasis via mediating degradation of NFκb negative regulator PPM1B. Am J Transl Res 8: 405-418, 2016.
67. Yang C, Wu J, He H and Liu H: Small molecule NSC1892 targets the CUL4A/4B-DDB1 interactions and causes impairment of $CRL4^{DCAF4}$ E3 ligases to inhibit colorectal cancer cell growth. Int J Biol Sci 16: 1059-1070, 2020.
68. Kim KT, Lee MH, Shin SJ, Cho I, Kuk JC, Yun J and Choi YY: Decorin as a key marker of desmoplastic cancer-associated fibroblasts mediating first-line immune checkpoint blockade resistance in metastatic gastric cancer. Gastric Cancer 28: 12-26, 2025.
69. Ieranò C, Righelli D, D'Alterio C, Napolitano M, Portella L, Rea G, Auletta F, Santagata S, Trotta AM, Guardascione G, *et al*: In PD-1+ human colon cancer cells NIVOLUMAB promotes survival and could protect tumor cells from conventional therapies. J Immunother Cancer 10: e004032, 2022.
70. Ye L, Zhang T, Kang Z, Guo G, Sun Y, Lin K, Huang Q, Shi X, Ni Z, Ding N, *et al*: Tumor-infiltrating immune cells act as a marker for prognosis in colorectal cancer. Front Immunol 10: 2368, 2019.
71. Chen Y, Zhao B and Wang X: Tumor infiltrating immune cells (TIICs) as a biomarker for prognosis benefits in patients with osteosarcoma. BMC Cancer 20: 1022, 2020.
72. Qin Y, Liu Y, Xiang X, Long X, Chen Z, Huang X, Yang J and Li W: Cuproptosis correlates with immunosuppressive tumor microenvironment based on pan-cancer multiomics and single-cell sequencing analysis. Mol Cancer 22: 59, 2023.
73. Zheng K, Hai Y, Chen H, Zhang Y, Hu X and Ni K: Tumor immune dysfunction and exclusion subtypes in bladder cancer and pan-cancer: A novel molecular subtyping strategy and immunotherapeutic prediction model. J Transl Med 22: 365, 2024.

74. Hu Y, Zheng M, Wang S, Gao L, Gou R, Liu O, Dong H, Li X and Lin B: Identification of a five-gene signature of the RGS gene family with prognostic value in ovarian cancer. Genomics 113: 2134-2144, 2021.
75. Yang Z, Wei X, Pan Y, Xu J, Si Y, Min Z and Yu B: A new risk factor indicator for papillary thyroid cancer based on immune infiltration. Cell Death Dis 12: 51, 2021.
76. Yamamoto H and Hirasawa A: Homologous recombination deficiencies and hereditary tumors. Int J Mol Sci 23: 348, 2021.
77. Villacampa G, Llop-Guevara A, Filmann N, Herencia-Ropero A, Fasching PA, Karn T, Marmé F, Klare P, Müller V, Stefek A, *et al*: RAD51 testing in patients with early HER2-negative breast cancer and homologous recombination deficiency: A Post-Hoc analysis of the GeparOLA trial. Clin Cancer Res 31: 808-814, 2025.
78. Tao S, Pu Y, Yang EJ, Ren G, Shi C, Chen LJ, Chen L and Shim JS: Inhibition of GSK3β is synthetic lethal with FHIT loss in lung cancer by blocking homologous recombination repair. Exp Mol Med 57: 167-183, 2025.
79. Wagener-Ryczek S, Merkelbach-Bruse S and Siemanowski J: Biomarkers for homologous recombination deficiency in cancer. J Pers Med 11: 612, 2021.
80. van der Wiel AMA, Schuitmaker L, Cong Y, Theys J, Van Hoeck A, Vens C, Lambin P, Yaromina A and Dubois LJ: Homologous recombination deficiency scar: Mutations and beyond-implications for precision oncology. Cancers (Basel) 14: 4157, 2022.
81. Hong CS, Ho W, Zhang C, Yang C, Elder JB and Zhuang Z: LB100, a small molecule inhibitor of PP2A with potent chemo- and radio-sensitizing potential. Cancer Biol Ther 16: 821-833, 2015.
82. Zhou X, Ying H, Sun Y, Zhang W, Luo P, Zhu S and Zhang J: Homologous recombination deficiency (HRD) is associated with better prognosis and possibly causes a non-inflamed tumour microenvironment in nasopharyngeal carcinoma. J Pathol Clin Res 10: e12391, 2024.
83. Hong L, Li J and Shao W: A risk model developed based on homologous recombination deficiency genes for evaluating the drug sensitivity and prognostic prediction of lung adenocarcinoma. Curr Med Chem 32: 6847-6866, 2025.
84. Liu C, Qian X, Yu C, Xia X, Li J, Li Y, Xie Y, Gao G, Song Y, Zhang M, *et al*: Inhibition of ATM promotes PD-L1 expression by activating JNK/c-Jun/TNF-α signaling axis in triple-negative breast cancer. Cancer Lett 586: 216642, 2024.
85. Deng J, Zhang T, Liu F, Han Q, Li Q, Guo X, Ma Y, Li L and Shao G: CRL4-DCAF8L2 E3 ligase promotes ubiquitination and degradation of BARD1. Biochem Biophys Res Commun 611: 107-113, 2022.
86. Wang Z, Zhao Y and Zhang L: Emerging trends and hot topics in the application of multi-omics in drug discovery: A bibliometric and visualized study. Current Pharmaceutical Analysis 21: 20-32, 2024.
87. Chen J, Lin A and Luo P: Advancing pharmaceutical research: A comprehensive review of cutting-edge tools and technologies. Current Pharmaceutical Analysis 21: 1-19, 2024.
88. Liu JL, Yang M, Bai JG, Liu Z and Wang XS: 'Cold' colorectal cancer faces a bottleneck in immunotherapy. World J Gastrointest Oncol 15: 240-250, 2023.